Utrecht University

Graduate school of natural sciences

Institute for theoretical physics

From Relativity to Beyond: Orbital Shifts in Extreme Mass Ratio Inspirals under Modified Gravity

Erik Mollers

December 2024

Master's thesis

under the supervision of

Dr. Tanja Hinderer
Iris van Gemeren MSc.
Dr. Elisa Chisari

Utrecht University

Abstract

General Relativity has revolutionized our understanding of gravity, yet challenges remain. Its incompatibility with quantum mechanics and the unresolved nature of singularities in high-density regimes highlight the need for modifications. These modifications might manifest in the strong-gravity domain of black holes and compact objects or become relevant only at Planck-scale phenomena. Gravitational waves provide a unique opportunity to test modified gravity theories in the strong-gravity regime, especially with next-generation high-precision detectors. However, detecting these effects requires robust theoretical models, beginning with an understanding of how black hole binaries evolve in modified gravity theories.

This thesis investigates extreme mass ratio inspirals, systems in which a stellar-mass object orbits a supermassive black hole. These inspirals evolve over long timescales, allowing cumulative deviations from General Relativity to emerge. Two modified gravity theories, dynamical Chern-Simons (dCS) and scalar Gauss-Bonnet (sGB), are explored. A geometric framework for dynamical systems is introduced to analyze resonances, which are especially sensitive to perturbations. Additionally, an effective potential approach is employed to examine phase-space regions of bound orbits in extreme mass ratio binaries. We found that dCS enlarges the region of bound orbits aligned with the spin of the supermassive black hole and shifts all orbits inward. In contrast, sGB increases the regions of bound orbits both aligned and counter-aligned with the spin, while shifting all orbits outward. These findings suggest trends in orbital dynamics that could inform future observational tests of modified gravity theories.

Contents

Chapter 1

Introduction

Gravity, the fundamental interaction governing the motion of celestial bodies, was profoundly redefined in 1915 when Albert Einstein published his theory of General Relativity (GR) [1]. This groundbreaking framework describes gravity not as a force but as the curvature of spacetime caused by mass and energy. GR has since achieved remarkable success, accurately predicting phenomena such as Mercury's orbital precession, the bending of light, and even the existence of black holes. Yet, despite its empirical triumphs [2], GR faces fundamental challenges. at the forefront lie the problems one encounters when one tries to combine GR with the framework of quantum field theories.

The early 20th century was a transformative period for physics. Alongside the development of GR, the quantum revolution reshaped our understanding of the microscopic world, culminating in the standard model of particle physics [3]. At the same time, GR describes macroscopic phenomena with unparalleled precision. Much work has been done to combine these two frameworks, but still, problems remain [4, 5]. These problems raise questions about GR's completeness, particularly in regimes of extreme curvature, such as near black hole singularities or during the initial moments of the universe's existence.

To address these challenges, various modified theories of gravity have been proposed, extending GR's framework to include new fields, higher-order curvature corrections, or other enhancements that become significant in strong-field regions [6]. Modified theories of gravity are further motivated by low-energy limits of speculative quantum gravity frameworks, such as string theory and loop quantum gravity, which naturally incorporate new fields and higher-order curvature corrections [7, 8, 9, 10]. However, direct experimental probes of strong-gravity regions remained elusive in the twentieth century. Black holes and compact objects, where these modifications are most prominent, are inherently difficult to study through traditional astronomical means.

The advent of gravitational wave (GW) astronomy has opened a new window into these extreme environments. GW, ripples in spacetime produced by cataclysmic astrophysical events, e.g. during the merger of two black holes, were first directly detected in 2015 by the LIGO-VIRGO detectors [11]. GWs were predicted by GR nearly a hundred years before they were experimentally

measured, and they encode the nature of the cataclysmic events by which they are produced. Since these events are mainly black hole or other compact object mergers, these GWs are actually encoding the nature of gravity in high curvature regimes. Projects such as the Laser Interferometer Space Antenna (LISA) [12] and the Einstein Telescope [13] promise to push this frontier further, enabling high-precision detections of sources like merging black holes, neutron stars or even more exotic compact objects. These next-generation observatories offer a unique opportunity to test modified gravity theories in regimes previously inaccessible to observation.

A key focus of LISA will be extreme mass ratio inspirals (EMRIs) [12], binary systems where a stellar-mass object spirals into a supermassive black hole ($10^5 - 10^6 M_\odot$), which lie at the center of galaxies. The rate at which astrophysical EMRIs occur is very uncertain, leading to a wide range of possible yearly EMRI detections by LISA. However, reasonable models estimate that LISA will detect tens to almost a thousand EMRI events per year [14].

These EMRIs will be the focus of our work, as they are particularly promising for probing modifications to GR. They spend many more orbits in the inspiral phase which allows even subtle deviations from GR to accumulate, offering a sensitive laboratory for testing modified gravity [15]. Over small timescales, the stellar mass object follows the geodesics of the supermassive black hole, while over longer timescales the gravitational radiation reaction causes orbits to shrink. Furthermore, for accurate calculations one must consider the gravitational self-force of the stellar mass object, which represents the interaction with its own spacetime curvature [16]. We aim to scope out possible new phenomena and will not include the gravitational self-force in our initial exploration.

This thesis investigates how the orbital dynamics of EMRIs are modified under two specific gravity theories: dynamical Chern-Simons (dCS) gravity [17] and scalar Gauss-Bonnet (sGB) gravity [18]. These modifications both add a quadratic curvature term coupled to a dynamic scalar field to the action. An attractive feature of these quadratic curvature terms, is that they have been shown to render the quantum field theorie normalizable, solving a fundamental problem encountered when combining the two frameworks [19].

Two complementary approaches are employed. A geometric framework is developed to examine resonances, which are particularly sensitive to perturbations [20, 15]. Additionally, an effective potential framework [21] is utilized to investigate the phase-space regions of bound geodesic orbits around supermassive black holes. Together, these methods aim to identify distinct dynamical signatures of dCS and sGB gravity, contributing to the broader effort of testing GR through gravitational wave observations.

The thesis is structured as follows: Chapter 2 introduces the mathematical preliminaries for constructing the geometric framework, assuming a basic familiarity with multivariable calculus. Chapter 3 develops the geometric framework to analyze resonances in dynamical systems. Chapter 4 explores various modifications to GR, introducing the two gravity theories under study. Chapter 5 outlines conserved quantities in EMRIs and constructs the effective potential

framework. The analysis of bound orbits using this framework is presented in Chapter 6. Finally, Chapter 7 discusses the implications of these findings, while Chapter 8 highlights directions for future research.

Chapter 2

Mathematical preliminaries

This chapter establishes the mathematical foundation necessary to investigate the framework for dynamical systems, introduced in Chapter 3, which can be used to study EMRIs. Assuming a working knowledge of multivariable calculus, we focus on the concepts most relevant to understanding the dynamical framework. Rather than providing a comprehensive treatment of these topics, we aim to offer a concise overview to facilitate understanding. Readers seeking greater depth are encouraged to consult specialized textbooks. For those well-versed in advanced mathematics, this chapter may be skipped, utilizing it as a reference when needed.

In Sec. 2.1, we will give a brief overview of two different mathematical disciplines; group theory and topology. We then delve into differential geometry, beginning in Sec. 2.2 with an introduction to smooth manifolds, topological spaces that locally resemble the familiar $\mathbb{R}^n$ from multivariable calculus but may have entirely different global properties. Next, in Sections 2.3 and 2.4, we will discuss how to generalize the notions of vector and covector spaces, respectively. In the latter, we will also introduce differential forms, which are critical for performing calculus on manifolds. Finally, in Sec. 2.5, we examine Lie groups, which are mathematical objects that combine the smooth structure of manifolds with the algebraic properties of groups.

In this chapter and throughout the remainder of this work, we adopt the Einstein summation convention unless stated otherwise. Repeated indices, one raised and one lowered, are implicitly summed over their range. For example, $v^i\partial_i$ is understood to mean $\sum_{i=1}^{\dim} v^i\partial_i$, where dim depends on the context of the index i. In this chapter, dim will often be the dimension of the manifold.

2.1 Groups and topology

Most people know intuitively what a group is, but what is the mathematical definition of a group? This is precisely what the beginning of this section will cover. In Sec. 2.1.1 we will introduce groups within mathematics. Next, In Sec. 2.1.2 we will introduce group generators, a minimal amount of group elements from which the entire group can be generated.

Finally, we will cover a concept from topology, which is a sub-discipline of mathematics that asks: which spaces can be continuously deformed into one another? A continuous deformation constitutes anything that does not tear, opens or closes holes or glues surfaces together. As such, from a topologist's viewpoint, a coffee mug and a donut are the same objects. Two of such same objects are said to be homeomorphic to each other, and there exists some homeomorphism between them. Homeomorphisms preserve topological properties of a space, one of such properties is the first homotopy group, which is also sometimes called the fundamental group in the literature. In Sec. 2.1.3 we will develop the general idea behind the first homotopy group. We will not at all attempt to be mathematically rigorous here, as the general idea is all we need.

2.1.1 Mathematical groups

A group is mathematically defined as a set of elements together with a group operation, that is closed and associative. Closure of the group action means that for every element a and b of the group G, we have $a \cdot b = c$, where c is again an element of the group G. Associativity of the group action entails:

$$(a \cdot b) \cdot c = a \cdot (b \cdot c), \tag{2.1}$$

for all elements $a, b, c \in G$. Furthermore, we require that the set has an identity element e, that satisfies:

$$a \cdot e = e \cdot a = a, \tag{2.2}$$

for every element $a \in G$. Finally, all elements a of the group must also have an inverse element s^{-1}, that is contained in the group, and which satisfies:

$$a \cdot a^{-1} = a^{-1} \cdot a = e. \tag{2.3}$$

Some examples of groups are the real numbers $\mathbb{R}$, or the integers $\mathbb{Z}$, paired with addition.

2.1.2 Group generators

Let a be an element of our group G and n an integer. We define na to be [22]:

$$na = a \cdot \pm a \cdot ... \cdot \pm a, \tag{2.4}$$

where the pluses are for positive integers, the minus for negative, and the group operation appears n times. We now define the set of generators of a group G as the minimal set of elements $\{a^i\}$, which generates each element b of the group as:

$$b = n_i a^i, \tag{2.5}$$

for some set of integers $\{n_i\}$. For example, $\mathbb{Z}$, under addition, has as generator either 1 or -1, and $\mathbb{Z}^2$, under addiction, has the generators $(1, 0)$ and $(0, 1)$.

2.1.3 First homotopy group

Take a look at Fig. 2.1, here we see two similar looking topological spaces, $\mathcal{M}$ and $\mathcal{M}_o$. The only difference between these two spaces is that the latter has a hole in it, while the former does not. These spaces are thus not homeomorphic to each other. In order to describe their difference, in a more systematic way, we introduce the concept of two functions being homotopic. If F_1 and F_2 are both functions from a topological space $\mathcal{X}$ into a topological space $\mathcal{Y}$, we say that these functions are homotopic if their image can be continuously deformed into each other [22]. This produces an equivalence class of functions, where all functions that are homotopic belong to the same homotopy class.

Now, take $\mathcal{X}$ to be the unit circle, and $\mathcal{Y}$ to be the space where we want to define a topological property. In Fig. 2.1a, we have drawn the map γ, which maps the unit circle into $\mathcal{M}$. This map γ, just like any other map from the unit circle into $\mathcal{M}$, can be continuously deformed into a point, i.e., all these maps are homotopic. The situation is different in Fig. 2.1b, where α and α' cannot be continuously deformed into each other due to the presence of the hole in $\mathcal{M}_o$. Each homotopic equivalence class of $\mathcal{M}_o$ can be represented by an integer number; positive numbers for the number of clockwise rotations around the hole, negative numbers for anti-clockwise rotations, and 0 means no rotations. If we take the set of all equivalence classes of the topological space $\mathcal{M}_o$, and define addition as the group operation, we get the first homotopy group $\Pi_1(\mathcal{M}_o)$ [22].

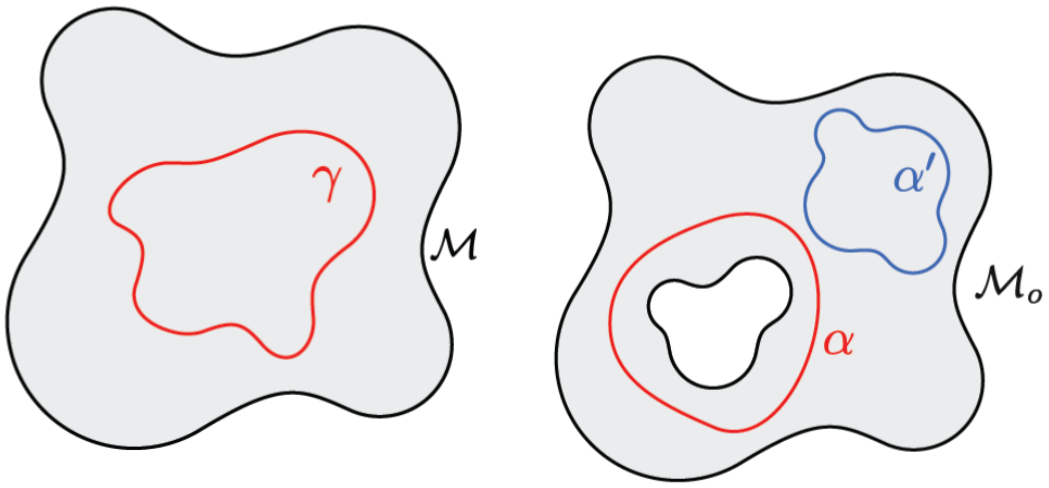

(a) $\mathcal{M}$ **(b)** $\mathcal{M}_o$

Figure 2.1: Comparison of Two Topological Spaces: (a) The space $\mathcal{M}$ without a hole, showing the red image of the map γ mapping the unit circle; (b) The space $\mathcal{M}_o$ with a hole, displaying the red image of the map α and the blue image of the map α', both mapping the unit circle.

2.2 Smooth manifolds

Having introduced groups and the notion of the first homotopy group, we will now devote this section to developing the idea of a smooth manifold. Smooth manifolds $\mathcal{M}$ are the objects studied within differential geometry. In simple terms, a smooth manifold is an object that locally looks like an Euclidean space $\mathbb{R}^n$, but it could globally be very different. Furthermore, we can perform calculus on these objects.

We will start in Sec. 2.2.1 by defining what a coordinate chart is. This will help us define, more rigorously, how smooth manifolds locally look like a Euclidean space. Next, in Sec. 2.2.2 we will state when a function between two Euclidean spaces is a diffeomorphism. In Sec. 2.2.3, we will use the concept of a diffeomorphism, to define an inclusion criterion of which coordinate charts we can use to describe a manifold locally, such that we can perform calculus. Subsequently, in Sec. 2.2.4 we will explain how to perform calculus on functions between two different manifolds. Finally, in Sec. 2.2.5 we will work out an example of a manifold, the N-torus T^N.

2.2.1 Coordinate charts

What we mean by the fact that smooth manifolds locally look like $\mathbb{R}^n$, where n is called the dimension of $\mathcal{M}$, is that we have a collection of coordinate maps φ_i, that are homeomorphisms between open subsets U_i of $\mathcal{M}$ and open subsets V_i of $\mathcal{R}^n$. These coordinate maps allow us to identify a point p, of the manifold $\mathcal{M}$, with the local coordinates of V_i [23].

$$\varphi_i(p) = (x^1, x^2, ..., x^n) \in V_i, \quad p \in \mathcal{M}. \tag{2.6}$$

The combination (U_i, φ_i) is called a coordinate chart, consisting of the coordinate map and its domain. An example of how two such coordinate charts look like is depicted in Fig. 2.2. A collection of coordinate charts, whose collective domain completely cover $\mathcal{M}$, is called an atlas of $\mathcal{M}$. We know how to perform calculus on the Euclidean spaces, and we would like to lift this notion to a manifold. The logical way of doing this is by looking at the composite function:

$$F \circ \varphi_i^{-1} : \mathbb{R}^n \to \mathbb{R}, \tag{2.7}$$

to make statements about the function F on our manifold. In order to ensure that the conclusions about the functions F, are independent of the specific chart we used, we will need some extra structure on the atlas. To this end, we will now first define what a diffeomorphism is.

2.2.2 Diffeomorphisms in Euclidean spaces

Assume there exists some map f, that maps one Euclidean space into another:

$$f : \mathbb{R}^n \to \mathbb{R}^m. \tag{2.8}$$

The map is called smooth, if the component functions have continuous partial derivatives to all orders [23]. Furthermore, assume that f is a bijective map, meaning that it is both injective and surjective, where the former means that all elements of $\mathbb{R}^m$ have at most one element of $\mathbb{R}^n$ mapped onto them, and the latter means that all elements of $\mathbb{R}^m$ are in the image of our map f. If the map f is a bijection then there exists an inverse map f^{-1}. If now both f and its inverse are smooth, then f is a diffeomorphism.

2.2.3 Transition functions

The function $\varphi_2 \circ \varphi_1^{-1}(U_1 \cap U_2)$ is called the transition function from φ_1 to φ_2, as is shown in Fig. 2.2.

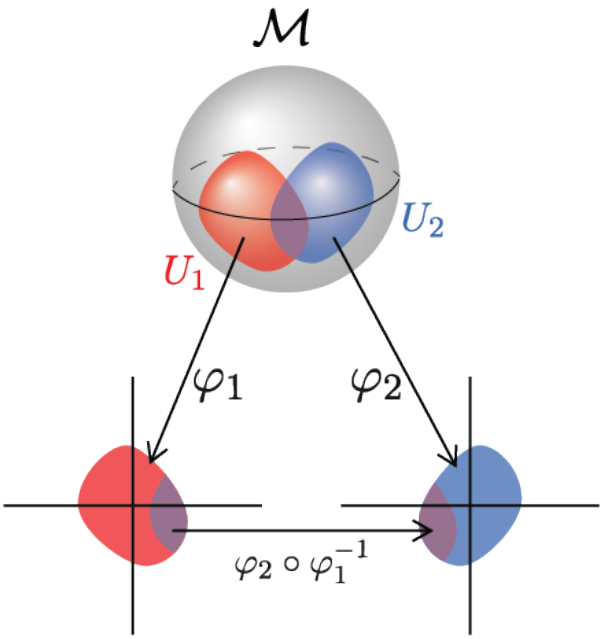

Figure 2.2: A spherical manifold $\mathcal{M}$ is depicted, together with two of its charts (U_1, φ_1) and (U_2, φ_2). The domains of these charts have some overlap, the transition function $\varphi 2 \circ \varphi_1^{-1}$, from the first to the second chart is also shown.

To ensure that the statements about objects on the manifold are independent of the chart we use, we limit the coordinate charts that we add to the atlas. We can only include charts in our atlas whose transition functions are diffeomorphisms, or whose domains have no overlap; this is now called a smooth atlas.

2.2.4 Functions between manifolds

The final objects we will introduce in this section, are functions F between two manifolds $\mathcal{M}$ and $\mathcal{N}$. Assume that $\mathcal{M}$ and $\mathcal{N}$ have covering charts (U_i, φ_i) and (W_i, ψ_i) respectively. Statements about the function F, must again be made

with respect to the charts of both manifolds, such that we can use the notion of calculus of Euclidean spaces. If the function:

$$\psi \circ F \circ \varphi^{-}1 \tag{2.9}$$

is smooth for all the charts we call F smooth. Likewise, if it is a diffeomorphism we call F a diffeomorphism, and we say that $\mathcal{M}$ is diffeomorphic to $\mathcal{N}$. From a differential geometry perspective, these manifolds are identical objects.

Throughout the rest of this thesis we will drop the smooth adjective, whenever we talk about a manifold it is assumed to be a smooth manifold with some smooth atlas. Whenever we talk about local coordinates on the manifold, we will often not explicitly specify the chart that we are working in.

2.2.5 An example: the N-torus

As an example, we will now work out the manifold structure of an N-torus. To this end, we will have to start with the unit circle S^1, since the N-torus is a product manifold of N unit circles. S^1 is a circle with a radius of one, i.e., it is given by the equation $x^2 + y^2 = 1$ in the xy-plane. We need at least two charts to cover the unit circle, since the circle itself is not homeomorphic to the real line. This means that we need to remove a point from the charts. An example of two charts that can form a smooth atlas are [22]:

$$\varphi_1^{-1} : \theta \mapsto \big(\cos(\theta), \sin(\theta)\big), \quad \theta \in (0, 2\pi), \tag{2.10a}$$

and

$$\varphi_2^{-1} : \theta \mapsto \big(\cos(\theta), \sin(\theta)\big), \quad \theta \in (-\pi, \pi). \tag{2.10b}$$

In this example, the first chart removes the point $(1, 0)$ from the circle, and the second chart removes the point $(-1, 0)$.

Now that we know how to form a smooth atlas for the unit circle, we turn to the description of a product manifold. If we have two manifolds, $\mathcal{M}$ an m-dimensional manifold with an atlas $\{(U_i, \varphi_i)\}$, and $\mathcal{N}$ an n-dimensional manifold an atlas $\{(V_j, \psi_j)\}$, the product manifold $\mathcal{M} \times \mathcal{N}$ will be an (m+n)-dimensional manifold with the atlas $\{(U_i \times V_J), (\varphi_i, \psi_j)\}$ [22]. Furthermore, any point in the product manifold can be written as (p, q), where p is a point in $\mathcal{M}$ and q is a point in $\mathcal{N}$. In local coordinates, the point (p, q) becomes:

$$(\varphi_i(p), \psi_j(q)) = (x_1, \cdots, x_m, y_1, \cdots, y_n), \tag{2.11}$$

which is a point in $\mathbb{R}^{m+n}$.

As mentioned before, an N-torus is a product manifold of N unit circles, a point in T^N is therefore given by $(\theta_1, \cdots, \theta_N)$, where each θ represents the angle of one of the unit circles. The 2-torus, also often just called torus, is the most famous example. The torus is often depicted as a donut as is shown in Fig. 2.3, which is an embedding of the torus in 3-dimensional space. A feature of this embedding is that the torus looks curved. If we would however look at the torus

embedded in a 4-dimensional space the torus will be flat [22]. This is however hard to depict, which is why usually the former embedding is chosen.

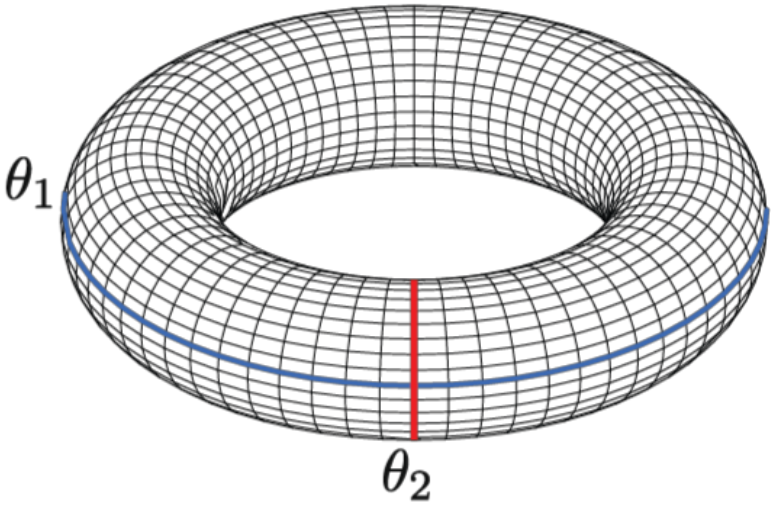

Figure 2.3: A torus embedded in a 3-dimensional space is depicted. The torus is a product manifold of two unit circles. A point on the torus is given by (θ_1, θ_2), where θ_1 is a point in the first unit circle and θ_2 is a point in the second unit circle.

2.3 Tangent spaces and vector fields

Now that we know what a smooth manifold is, it is time to define tangent spaces. A tangent space $\mathcal{T}_p\mathcal{M}$ is, as the name suggests, the space that contains all tangent vectors at the point $p \in \mathcal{M}$. A vector field is a map that maps each point on the manifold into a tangent vector. This section will be devoted to developing both of these related concepts.

We will start in Sec. 2.3.1, by explaining different ways of looking at tangent vectors: the geometric image, which may be familiar from all the way back in high school physics, and viewing vectors as taking directional derivatives of smooth functions. In Sec. 2.3.2 we explain how a smooth function between two manifolds naturally induces a map between their respective tangent spaces. This induced map can be used to push tangent vectors in the same direction as the smooth function, and is hence called the push forward. In Sec. 2.3.3 we will introduce vector fields, and explain what an integral curve of a vector field is. Next, in Sec. 2.3.4 we will explain how each vector field creates a flow on the manifold, which is given by the collection of all its integral curves. Subsequently, We will add a group structure on top of these flows, turning it into the one-parameter group of transformations. Finally, in Sec. 2.3.5 we will introduce the concept of a Lie bracket. A Lie bracket combines two vector fields, in a specific way, to obtain another vector field on the manifold.

2.3.1 Tangent vectors

There are multiple ways of describing tangent vectors. Geometrically, they are easiest to visualize if we are looking at a two-dimensional manifold. In this case we can view the tangent vectors $\mathbf{v}$ as arrows that are tangent to the surface of our manifold and whose origin coincides with the point p. The tangent space $\mathcal{T}_p\mathcal{M}$, can be visualized as a two-dimensional plane that is tangent to the manifold. An example of this geometric image is shown in Fig. 2.4.

Another way to look at tangent vectors is as maps from smooth functions on the manifolds to the real numbers; the directional derivative of the function in the direction of the tangent vector. Here a smooth function is defined in the sense of Eq. 2.7. This way of looking at tangent vectors, naturally leads to the following formula in local coordinates [23]:

$$\mathbf{v} = v^i \frac{\partial}{\partial x^i}\bigg|_p, \tag{2.12}$$

where v^i are called the components of $\mathbf{v}$ with respect to the local coordinates $\{x^i\}$, and $\frac{\partial}{\partial x^i}$ are the coordinate basis vectors. This gives the directional derivative, of a function F along $\mathbf{v}$, in local coordinates as:

$$\mathbf{v}(F) = v^i \frac{\partial F \circ \varphi^-1}{\partial x^i}\big(\varphi(p)\big). \tag{2.13}$$

2.3.2 Push forward

Smooth functions F, between two manifolds $\mathcal{M}$ and $\mathcal{N}$, naturally induce a map F_* between their respective tangent spaces. We will refer to this map as the push forward, since it can push tangent vectors forward; in the literature it is also often called the differential map of F [22]:

$$F_* : \mathcal{T}_p\mathcal{M} \to \mathcal{T}_{F(p)}\mathcal{N}. \tag{2.14}$$

If g is a smooth function from $\mathcal{N}$ to $\mathbb{R}$, then $g \circ F$ is a smooth function from $\mathcal{M}$ to $\mathbb{R}$, meaning that we can take directional derivatives with some tangent vector $\mathbf{v} \in \mathcal{T}_p\mathcal{M}$. This is exactly how the push forward works:

$$(\mathbf{F}_*\mathbf{v})(g) = \mathbf{v}(g \circ F). \tag{2.15}$$

If we have local coordinates $p = (x^1, ..., x^m)$ in $\mathcal{M}$, and $F(p) = (y^1, ..., y^n)$ in $\mathcal{N}$, we can express the components w^j of $(\mathbf{F}_*\mathbf{v})$ in terms of the components v^i of $\mathbf{v}$ as [22]:

$$w^j = v^i \frac{\partial y^j}{\partial x^i} \tag{2.16}$$

2.3.3 Vector fields

We are now in a position to define vector fields. A vector field $\mathbf{Y}$ is a smooth map, that maps each point p of the manifold into the tangent vector $\mathbf{Y_p}$. In local coordinates this entails that the components of a vector field are now smooth functions on the manifold. i.e., we have:

$$\mathbf{Y_p} = Y^i(p)\frac{\partial}{\partial x^i}\bigg|_p . \tag{2.17}$$

An integral curve $\rho(t)$ of this vector field is a curve whose tangent vector at the point $p = \rho(t_0)$ is $\mathbf{Y_p}$. This is geometrically depicted in Fig. 2.4. In local coordinates, this becomes [22]:

$$\frac{\mathrm{d}x^i}{\mathrm{d}t} = Y^i\big(\rho(t_0)\big) \tag{2.18}$$

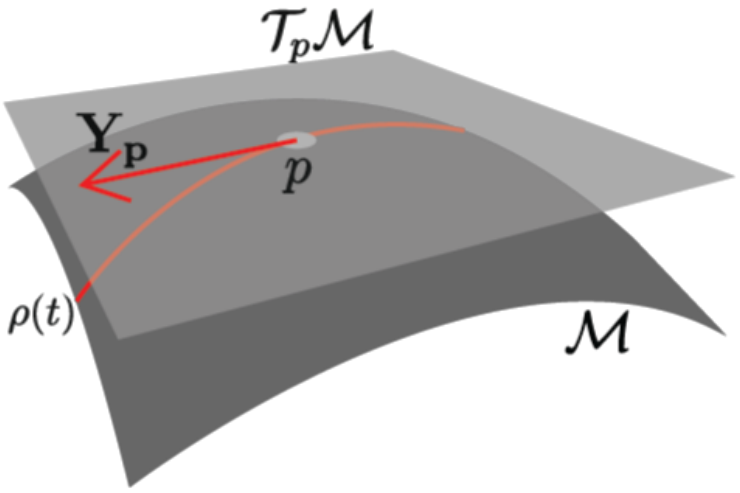

Figure 2.4: An integral curve $\rho(t)$ of the vector field $\mathbf{Y}$ is shown, together with its tangent vector at the point $p = \rho(t_0)$.

2.3.4 Flows and the one-parameter group of transformations

We will now take a closer look at the integral curves, whereby $\rho(t, p)$ we denote the integral curve of $\mathbf{Y}$ that passes the point p at $t = 0$. If we denote its local coordinate representation by $\rho^i(t, p)$, we get:

$$\frac{\mathrm{d}}{\mathrm{d}t}\rho^i(t,p) = Y^i\big(\rho(t,p)\big). \tag{2.19}$$

This is an ordinary differential equation with the initial condition $\rho^i(0, p) = x^i$. Existence and uniqueness theorems of ODEs guarantee that there exists unique integral curves that solve Eq. 2.19. Taking the collection of all these curves

gives a flow on the manifold that is generated by the vector field $\mathbf{Y}$. Formally speaking, it is a map $\rho : \mathbb{R} \times \mathcal{M} \to \mathcal{M}$, informally speaking, it tells each point of the manifold where to move to, creating a flow in the manifold.

Another way to look at the flow is by fixing some t in $\mathbb{R}$. This way $\rho_t(p)$ becomes a diffeomorphism from $\mathcal{M}$ to $\mathcal{M}$. We can add a group structure on these diffeomorphisms by taking note of the following rules: $\rho_t \cdot \rho_s = \rho_{t+s}$, ρ_0 is the identity element, and the inverse $(\rho_t)^{-1}$ is equal to ρ_{-t}. This group is called the one-parameter group of transformations. If we look at transformations by an infinitesimal ϵ, we find [22]:

$$\rho_\epsilon^i(p) = x^i + \epsilon Y^i(p), \tag{2.20}$$

hence, the vector field $\mathbf{Y}$ is called the infinitesimal generator of this transformation

2.3.5 Lie brackets

Just as tangent vectors, vector fields act as derivations on smooth functions. As derivations, vector fields satisfy the product rule. i.e., if we have two smooth functions f and g, and a vector field $\mathbf{Y}$, we get [23]:

$$\mathbf{Y}(fg) = \mathbf{Y}(f)g + f\mathbf{Y}(g). \tag{2.21}$$

It is interesting to think about taking combinations of vector fields to create a new vector field on the manifold. If we let a vector field $\mathbf{Y}$ act on the function f, we get back another function $\mathbf{Y}(f)$, which is a derivation of f. Next, we could let another vector field $\mathbf{Z}$ act upon this function $\mathbf{Y}(f)$, and ask ourselves: is this still a derivation? We find:

$$\mathbf{Z}\big(\mathbf{Y}(fg)\big) = \mathbf{Z}\big(\mathbf{Y}(f)g + f\mathbf{Y}(g)\big) \neq \mathbf{ZY}(f)g + f\mathbf{ZY}(g). \tag{2.22}$$

This means that $\mathbf{ZY}$ does not satisfy the product rule, due to the additional cross terms that we get. Hence, it is not a derivation, and also not a vector field. Since the same cross terms appear, whether we first act with $\mathbf{Y}$ or with $\mathbf{Z}$, taking the difference of the two would cancel the troublesome terms, therefore, this combination is a vector field. This new vector field is called the Lie bracket of $\mathbf{Z}$ and $\mathbf{Y}$, and is denoted as:

$$[\mathbf{Z}, \mathbf{Y}] = \mathbf{ZY} - \mathbf{YZ}. \tag{2.23}$$

2.4 Cotangent spaces and forms

Just as in linear algebra, we can define a dual vector space, which in differential geometry is called the cotangent space $\mathcal{T}_p^*\mathcal{M}$. Elements of the cotangent space are called cotangent vectors, or one-forms in the context of differential forms. This section will be devoted to developing the necessary theory around cotangent spaces for the rest of our work.

We will start in Sec. 2.4.1 by explaining what a cotangent vector/one-form is, and provide some examples. In Sec. 2.4.2, we will state what a pullback is, which is analogous to the push forward. In Sec. 2.4.3, we will briefly introduce tensors. These are multilinear objects that map multiple vectors and cotangent vectors onto the real numbers. Subsequently, in Sec. 2.4.4 we will develop the concept of differential forms, totally antisymmetric tensors that map multiple vectors into the real numbers. We will generalize the concept of the differential of a function in Sec. 2.4.5. This generalization is called the exterior derivative and takes r-forms into (r+1)-forms. Next, in Sec. 2.4.6 we will introduce the interior product, which takes r-forms into (r-1)-forms. Finally, in Sec. 2.4.7 we will state Stokes' theorem, which is a generalization of the classic integral theorems in vector calculus.

2.4.1 Cotangent vectors (one-forms)

Cotangent vectors can be seen as linear maps from the tangent space into the real numbers. An example of such a one-form is the differential $\mathbf{df}$ of a function f. We already know that tangent vectors take directional derivatives of functions. We can use this to define the inner product between the one form $\mathbf{df}$ and a tangent vector $\mathbf{v_p}$ [22]:

$$\langle \mathbf{df}, \mathbf{v} \rangle = \mathbf{v}(f) = v^i \frac{\partial f}{\partial x^i}(p). \tag{2.24}$$

This naturally leads us to the following definition of the differential in local coordinates:

$$\mathbf{df} = \frac{\partial f}{\partial x^i} dx^i, \tag{2.25}$$

where $\frac{\partial f}{\partial x^i}$ are the components of this one form with respect to the local coordinates and dx^i is the dual coordinate basis. The dual basis satisfies the following relation:

$$\left\langle dx^i, \frac{\partial}{\partial x^j} \right\rangle = \frac{\partial x^i}{\partial x^j} = \delta^i_j. \tag{2.26}$$

From here on forward, we will denote the inner product between a one form ω and a vector $\mathbf{v}$ as:

$$\langle \omega, \mathbf{v} \rangle = \omega(\mathbf{v}) = \omega_i v^i \tag{2.27}$$

2.4.2 Pullback

In Sec. 2.3.2 we showed how a smooth function F, from a manifold $\mathcal{M}$ into the manifold $\mathcal{N}$, induces the push forward F_* between their respective tangent spaces. Similarly, this function induces a smooth map between the respective cotangent spaces:

$$F^* : \mathcal{T}_F(p)^*\mathcal{N} \to \mathcal{T}_p^*\mathcal{M}, \tag{2.28}$$

This map goes in the opposite direction of F, hence it is called the pullback. Globally, this map is defined using the inner product between the tangent and cotangent spaces. If we take $\omega \in \Omega(\mathcal{N})$ and $\mathbf{v} \in \mathcal{T}_p\mathcal{M}$, we get [22]:

$$F^*\omega(\mathbf{v}) = \omega(F_*\mathbf{v}) \tag{2.29}$$

2.4.3 Tensors

We can now define (r,m) tensors $\mathbf{T}$ on the manifold, which are multilinear objects that map r one-forms and m vectors into the real numbers. I.e. if we take r one-forms $\omega_1, ..., \omega_r$, and m vectors $\mathbf{v_1}, ..., \mathbf{v_m}$, we get:

$$\mathbf{T}(\omega_\mathbf{1}, ..., \omega_\mathbf{r}, \mathbf{v_1}, ..., \mathbf{v_m}) \in \mathbb{R}. \tag{2.30}$$

In local coordinates we can denote an (r,m) tensor as [22]:

$$\mathbf{T} = T^{i_1...i_r}_{j_1...j_m} \frac{\partial}{\partial x^{i_1}} \otimes ... \otimes \frac{\partial}{\partial x^{i_r}} \otimes dx^{j_1} \otimes ... \otimes dx^{j_m}, \tag{2.31}$$

where $\otimes$ is the usual tensor product. Some physical examples of tensors are the energy momentum tensor, spin currents, and the metric tensor.

2.4.4 Differential forms

Next, we will define r-forms, which are (0,r) tensors that are completely antisymmetric in all their indices. As it is conventional in the literature, we will denote the space in which these r-forms reside as $\Omega^r(\mathcal{M})$, where, as mentioned before, we identify the space of one-forms $\Omega(\mathcal{M})$ with the cotangent bundle $\mathcal{T}_p^*\mathcal{M}$. In order to define a coordinate basis for these r-forms, we have to first introduce the wedge product $\wedge$. This is defined as the completely antisymmetric tensor product. E.g. the coordinate basis of 2 forms is given by:

$$dx^i \wedge dx^j = dx^i \otimes dx^j - dx^j \otimes dx^i. \tag{2.32}$$

A general r-form ω can be projected onto local coordinates as [22] :

$$\omega = \frac{1}{r!}\omega_{i_1...i_r} dx^{i_1} \wedge ... \wedge dx^{i_r}, \tag{2.33}$$

where we note that the wedge product makes the r-form completely antisymmetric.

2.4.5 Exterior derivative

We saw before how the differential takes a function f, which can be seen as an 0-form, into the one-form $\mathbf{df}$. We generalize this operation d and call it the exterior derivative:

$$d : \Omega^r(\mathcal{M}) \to \Omega^{r+1}(\mathcal{M}). \tag{2.34}$$

In local coordinates, it acts on an r-form ω as [22]:

$$d\omega = \frac{1}{r!}\left(\frac{\partial}{\partial x^j}\omega_{i_1\ldots i_r}\right) dx^j \wedge dx^{i_1} \wedge \ldots \wedge dx^{i_r}. \tag{2.35}$$

Forms whose exterior derivative is zero are called closed, and forms that are the exterior derivative of a lower rank form are called exact. Note that since the partial derivatives commute, and we contract the components with an antisymmetric basis, applying the exterior derivative to a form twice gives zero. Therefore, exact forms are a subgroup of the closed forms.

2.4.6 Interior product

Lastly, we would like to introduce the interior product $\imath$. The interior product inserts a vector field into the first slot of an r-form, which therefore becomes an (r-1)-form. Take for example a 2-form ω, and a vector field $\mathbf{Y}$, the interior product is globally defined as [22]:

$$\imath_{\mathbf{Y}}\omega(..., ...) = \omega(\mathbf{Y}, ...), \tag{2.36}$$

or in local coordinates as:

$$\imath_{\mathbf{Y}}\omega = \frac{1}{(2-1)!} Y^i \omega_{ij} dx^j, \tag{2.37}$$

which is a one-form.

2.4.7 Stokes' theorem

Just as in calculus, we are able to integrate on a manifold. Here, we are mainly interested in Stokes' theorem, which is a generalization of the various vector calculus integration theorems. The general setting is the following: the natural objects to integrate over a k-dimensional surface are k-forms. Take a k-form ω and U a k-dimensional submanifold of $\mathcal{M}$, we can integrate ω over U as [22]:

$$\int_U \omega = \int_U f(p) dx^1 \wedge \cdots \wedge dx^k = \int_U f(x^1, \cdots, x^k) dx^1 \cdots dx^k, \tag{2.38}$$

where after the first equality, we substituted the local coordinate expression of a general k-form, and after the final equality we showed how to evaluate this integral in local coordinates. Admittedly, there are a lot of subtleties that we

skipped in this explanation, but this general idea is all that we need. For the interested reader, we recommend chapter 15 and 16 of [23].

Now we are in a position to state Stokes theorem. If ω is a (k-1)-form on $\mathcal{M}$, which is a k-dimensional manifold with a (k-1)-dimensional boundary $\partial\mathcal{M}$, the following equality holds [23]:

$$\int_{\mathcal{M}} d\omega = \int_{\partial\mathcal{M}} \omega, \tag{2.39}$$

where $d\omega$ is the exterior derivative of ω. Note that if the manifold has no boundary, then the right-hand-side vanishes.

2.5 Lie groups

Now that we know how to perform calculus on manifolds, we will introduce Lie groups. A Lie group is a manifold, together with a group operation that acts on all the points of the manifold and satisfies the conditions described in Sec. 2.1.1. Furthermore, both the group operation, and taking the inverse of a group element are smooth maps.

2.5.1 Lie algebras

If we take two elements g_1 and g_2 of a Lie group G, the left translation is defined as follows [22]:

$$L_{g_2} g_1 = g_2 \cdot g_1. \tag{2.40}$$

Because the group operation of a Lie group is smooth, this left translation induces a push forward $L_{g_2 *}$, on the tangent spaces of the Lie group. This allows us to identify a special class of vector fields on a Lie group, vector fields that are invariant under left translation. I.e., we have:

$$L_{g_2 *} \mathbf{Y}_{g_1} = \mathbf{Y}_{g_2 \cdot g_1}, \tag{2.41}$$

for all g_1 and g_2 in G. Looking back at Eq. 2.16, we can write this equality in local coordinates as:

$$Y^i(g_1) \frac{\partial y^j(g_2 \cdot g_1)}{\partial y^i(g_1)} \frac{\partial}{\partial x^j}\bigg|_{g_2 \cdot g_1} = Y^i(g_2 \cdot g_1) \frac{\partial}{\partial x^i}\bigg|_{g_2 \cdot g_1}, \tag{2.42}$$

where $y^i(g)$ represents the local coordinates, of the point g, in our manifold G. We will denote the set of all left-invariant vector fields, of our Lie group G, as $\mathfrak{g}$, which is a subset of all the vector fields on the Lie group.

If we take two vector fields $\mathbf{Y}$ and $\mathbf{Z}$, both elements of $\mathfrak{g}$, then their Lie bracket is again a left-invariant vector field. We have [22]:

$$L_{g_2 *}[\mathbf{Z}, \mathbf{Y}]_{g_1} = \left[L_{g_2 *}\mathbf{Z}_{g_1}, L_{g_2 *}\mathbf{Y}_{g_1}\right] = [\mathbf{Z}, \mathbf{Y}]_{g_2 \cdot g_1}, \tag{2.43}$$

i.e., the left-invariant vector fields are closed under the Lie bracket. $\mathfrak{g}$ together with the Lie bracket, is called the Lie algebra of our Lie group G, which we will usually just denote as $\mathfrak{g}$.

These left-invariant vector fields are in one-to-one correspondence with the tangent vectors at the identity element of our Lie group. Take one of these tangent vectors ξ in $\mathcal{T}_eG$, we can define the left invariant vector field $\mathbf{Y}_\xi$ at point g as [22]:

$$\mathbf{Y}_\xi|_g = L_{g*}\xi. \tag{2.44}$$

This one-to-one correspondence is in fact a vector space isomorphism. We see that the left-invariant vector fields have a vector space structure with the same dimension as $\mathcal{T}_eG$, which has again the same dimension as the Lie group G.

2.5.2 Dual Lie algebra

Since $\mathfrak{g}$ has a vector space structure, as we discussed in the previous section, we can define a dual vector space $\mathfrak{g}^*$ called the dual Lie algebra. We will denote elements of $\mathfrak{g}^*$ by μ, which can be seen as linear maps from $\mathfrak{g}$ to the real numbers. By $\langle \cdot, \cdot \rangle$ we will denote the natural pairing between $\mathfrak{g}$ and $\mathfrak{g}^*$, i.e., if we have ξ in $\mathfrak{g}$ and μ in $\mathfrak{g}^*$ we get [24]:

$$\mu(\xi) = \langle \mu, \xi \rangle \quad \in \mathbb{R}. \tag{2.45}$$

Even though we identified $\mathfrak{g}$ with $\mathcal{T}_eG$ in the previous section, we should not think of $\mathfrak{g}^*$ as the cotangent space at the identity element of the Lie group G, and μ are no one-forms on G. Instead, we should think of it as an abstract vector space, of which we take the dual.

2.5.3 The exponential map

Just as any other vector field on a manifold, left invariant vector fields generate flows on our Lie group G. By $\rho_t(e)$, we denote a one-parameter group of transformations at the identity element of G, which is referred to in the literature as a one-parameter subgroup of G, since its image is a Lie subgroup [23]. We can now define the exponential map as the map that takes a left invariant vector field $\mathbf{Y}_\xi$ into the one-parameter subgroup that it generates at the identity element, i.e., we have [22]:

$$\exp(t\mathbf{Y}_\xi) = \exp(t\xi) = \rho_t^\xi(e), \tag{2.46}$$

with ξ in $\mathcal{T}_eG$. The exponential map is also schematically shown in Fig. 2.5

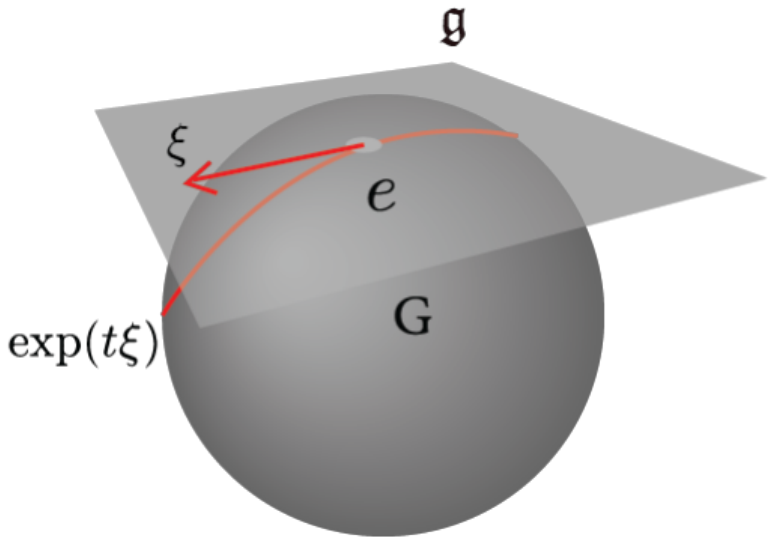

Figure 2.5: A Lie group G is depicted together with its Lie algebra $\mathfrak{g}$, which is isomorphic to $\mathcal{T}_eG$. In the Lie algebra, we drew the tangent vector ξ as a red arrow, while the image of the one-parameter subgroup that is generated by $\mathbf{Y}_\xi$ is depicted as a red line.

To get the full flow of the Lie group G, we can make use of the left translation invariance property. Where $\exp(t\xi)$ is just the integral curve of $\mathbf{Y}_\xi$ that starts at the origin. Since $\mathbf{Y}_\xi$ is left-invariant, left translation by $g \in G$ of its integral curve at the origin is again an integral curve of $\mathbf{Y}_\xi$, but this one starts at g. i.e.

$$\rho^\xi(t, g) = L_g \rho^\xi(t, e) = g \exp(t\xi). \tag{2.47}$$

2.5.4 Lie group actions on manifolds

In physical applications, it is quite common that a Lie group acts on a manifold. E.g., a rotation of the 3-dimensional Euclidean space $\mathbb{R}^3$ is mathematically described by the action of $SO(3)$ on $\mathbb{R}^3$, and the Poincare group acts on a Minkowski space to give rotations or Lorentz transformations. In this section, and throughout the rest of the thesis, we will focus on left group actions.

Mathematically, a group action Ψ is defined as a map from $G \times \mathcal{M}$ to $\mathcal{M}$ that satisfies the following two rules: $\Psi(e, p) = p$ for all points in $\mathcal{M}$ and $\Psi(g_1, \Psi(g_2, p)) = \Psi(g_1 \cdot g_2, p)$ for all g_1 and g_2 in G [22]. Looking at these rules, we note that we actually already encountered a group action before. The flows, which were described in Sec. 2.3.4, are a group action of the additive group $\mathbb{R}$.

We can make some further classification of these group actions. An action is called transitive if, for all p_1 and p_2 on $\mathcal{M}$, there is some g for which $\Psi(g, p_1) = p_2$. An action is called free if there are no group elements besides the identity element

that leave any point p in our manifold fixed. The orbit $G \cdot p$, of a point p under a group action, is defined as all the points in $\mathcal{M}$ that p get mapped to, i.e.

$$G \cdot p = \{\Psi(g, p) | g \in G\}. \tag{2.48}$$

Note that when the action is transitive, the orbit is equal to the entire manifold $\mathcal{M}$. The isotropy subgroup G_p is given by all the group elements g which keep the point e fixed:

$$G_p = \{g \in G | \Psi(g, p) = p\}. \tag{2.49}$$

When the action is free, the only element in the isotropy subgroup for any point p is the identity element.

In Eq. 2.47 we showed how ξ an element of the Lie algebra induces a flow in the corresponding Lie group. Similarly, by making use of the group action Ψ, ξ induces a flow in $\mathcal{M}$:

$$(t, p) \to \Psi\big(\exp(t\xi), p\big) = \exp(t\xi) \cdot p, \tag{2.50}$$

as is schematically shown in Fig. 2.6. In Sec. 2.3.4 we learned that flows are generated by vector fields. We call the infinitesimal generator of this flow $\xi_{\mathcal{M}}$, which is given by [22]:

$$\xi_{\mathcal{M}}|_p = \frac{\mathrm{d}}{\mathrm{d}t}\bigg|_{t=0} \exp(t\xi) \cdot p, \tag{2.51}$$

which is also depicted in Fig. 2.6. In this way, each Lie algebra element ξ naturally induces a vector field $\xi_{\mathcal{M}}$ on $\mathcal{M}$.

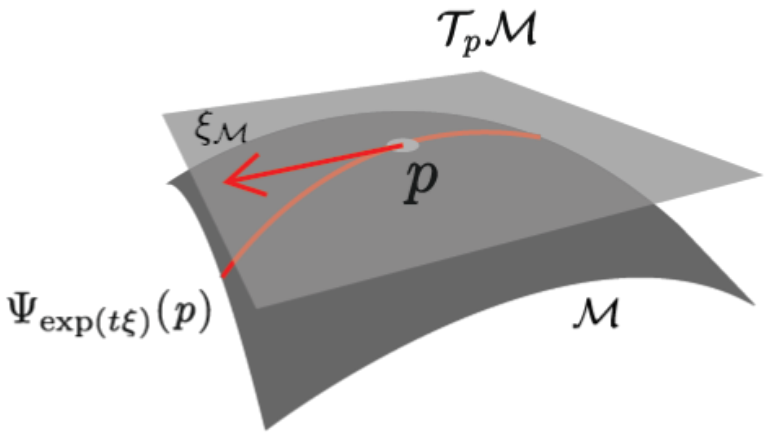

Figure 2.6: Geometric view of the induced vector field $\xi_{\mathcal{M}}$, and the induced flow $\Psi_{\exp(t\xi)}(p)$ by the Lie algebra element ξ.

2.5.5 Adjoint actions

Take g, h both elements of the Lie group G. We define the conjugation map C_h on G as [23]:

$$C_h(g) = h \cdot g \cdot h^{-1}. \tag{2.52}$$

This conjugation map is in fact a Lie group homomorphism because we have:

$$C_h(g_1 \cdot g_2) = C_h(g_1) \cdot C_h(g_2), \tag{2.53}$$

for all g_1 and g_2 in G. Furthermore, the map is smooth by smoothness of the Lie group action, therefore, it induces a push forward on $\mathcal{T}_eG$ which becomes a Lie algebra homomorphism:

$$Ad(g) = (C_g)_* : \mathfrak{g} \to \mathfrak{g}. \tag{2.54}$$

There is a different way of looking at this adjoint map. If we do not specify the group element, the adjoint map acts on, Ad becomes a map from the group G into $GL(\mathfrak{g})$ the group of linear transformation of $\mathfrak{g}$. This map is called the adjoint representation of G, and plays an important role in particle physics.

Lie groups can act on manifolds, as we saw in the previous section. The Lie algebra is isomorphic to $\mathcal{T}_eG$, which also has a manifold structure. For our application, we think about the adjoint representation as a group action of G on $\mathfrak{g}$, i.e., take g in G and ξ in $\mathfrak{g}$ and we get [25]:

$$Ad(g, \xi) = (C_g)_*\xi. \tag{2.55}$$

This action is called the adjoint action.

The adjoint representation is a representation of G on the vector space $\mathfrak{g}$. This naturally induces a representation of the G on the dual vector space $\mathfrak{g}^*$, which we will call the co-adjoint representation Ad^* of G, it is defined with the natural pairing as [24]:

$$\left\langle Ad^*(g)\mu, \xi \right\rangle = \left\langle \mu, Ad(g^{-1})\xi \right\rangle. \tag{2.56}$$

The g^{-1} on the right-hand-side of the definition is needed to ensure that it is a group homomorphism. We could again also look at Ad^* as an action of G on $\mathfrak{g}^*$, so we will also call this the co-adjoint action.

Chapter 3

Mathematical framework for dynamical systems

In this chapter, we construct a versatile framework to study dynamical systems, incorporating tools from various mathematical disciplines tailored to the study of EMRIs. We begin in Section 3.1 with a concise introduction to Hamiltonian mechanics, establishing the theoretical foundation for our discussion. Section 3.2 extends this understanding into the realm of symplectic geometry, offering a mathematically precise description of Hamiltonian systems. Action-Angle variables, a critical tool for analyzing certain systems, are introduced in Section 3.3. In Section 3.4, we present Marsden-Weinstein reduction, a method for reducing the dimension of the phase space by exploiting symmetries. Section 3.5 addresses the phenomenon of resonances and their role in dynamical systems. The chapter concludes with Section 3.6, where we investigate the impact of non-integrable perturbations on dynamical systems.

3.1 Introduction to Hamiltonian mechanics

A system with N particles is fully described by the positions q_α and momenta p_α of these particles. This set of 2N-variables form the coordinates of the phase space $\mathcal{M}$, which is a 2N-dimensional smooth manifold (see Sec. 2.2 for a recap on smooth manifolds). The time evolution of these coordinates is defined by the Hamiltonian $H(\mathbf{p}, \mathbf{q})$, a smooth function on $\mathcal{M}$ that maps 2N initial conditions onto the curve $(p_\alpha(t), q_\alpha(t)) \in \mathcal{M}$, $1 \leq \alpha \leq N$ by Hamilton's equations [26]:

$$\frac{\mathrm{d}q_\alpha}{\mathrm{d}t} = \frac{\partial H}{\partial p_\alpha}, \quad \frac{\mathrm{d}p_\alpha}{\mathrm{d}t} = -\frac{\partial H}{\partial q_\alpha}. \tag{3.1a}$$

These equations can be written in matrix form as:

$$\dot{\mathbf{x}} = \mathrm{J}\boldsymbol{\nabla} H, \quad \mathbf{x} \in \mathcal{M}, \quad \mathrm{J} = \begin{pmatrix} 0 & 1 \\ -1 & 0 \end{pmatrix}, \tag{3.1b}$$

where we are only considering Hamiltonian functions that are not explicitly time dependent.

Next, we will use the matrix J to define the Poisson bracket, which takes smooth functions on $\mathcal{M}$ into an infinite dimensional Lie algebra (see Sec. 2.5.1 for an introduction to Lie Algebras). For two smooth functions, F and G on $\mathcal{M}$ the Poisson bracket is given by:

$$\begin{aligned}\{F, G\} &= \langle \boldsymbol{\nabla} F | \mathrm{J} \boldsymbol{\nabla} G \rangle \\ &= \frac{\partial F}{\partial q_\alpha}\frac{\partial G}{\partial p^\alpha} - \frac{\partial G}{\partial q_\alpha}\frac{\partial F}{\partial p^\alpha}.\end{aligned} \tag{3.2}$$

Furthermore, for any smooth function $F(\mathbf{p}, \mathbf{q})$ on $\mathcal{M}$, that is not explicitly time dependent, we get:

$$\begin{aligned}\{F, H\} &= \frac{\partial F}{\partial q_\alpha}\frac{\mathrm{d}q_\alpha}{\mathrm{d}t} + \frac{\partial F}{\partial p_\alpha}\frac{\mathrm{d}p_\alpha}{\mathrm{d}t} \\ &= \frac{\mathrm{d}F}{\mathrm{d}t}.\end{aligned} \tag{3.3}$$

This shows us that the Hamiltonian is constant in time, since the Poisson bracket 3.2 is skew-symmetric.

What happens if we apply a coordinate transformation $\mathbf{x} \to \mathbf{y}$ to the phase space? The new equations of motion become:

$$\begin{aligned}\dot{\mathbf{y}} &= \Lambda \dot{\mathbf{x}} \\ &= \Lambda \mathrm{J} \boldsymbol{\nabla}_{\mathbf{x}} H \\ &= \Lambda \mathrm{J} \Lambda^T \boldsymbol{\nabla}_{\mathbf{y}} H,\end{aligned} \tag{3.4}$$

where Λ is the Jacobian of the coordinate transformation.

We see that the new equations of motion are Hamiltonian 3.1b if and only if the following condition holds: $\Lambda \mathrm{J} \Lambda^T = J$. Transformations that satisfy this condition are called canonical transformations. The above condition actually defines the Lie group $Sp(2N, R)$, called the symplectic group [27]. Thus, the natural way of formulating Hamiltonian mechanics is via symplectic geometry.

3.2 Geometric Hamiltonian systems

In this section we will start building the symplectic geometry framework for Hamiltonian systems. In Sec. 3.2.1 we begin by defining the symplectic form. The symplectic form gives the extra structure of symplectic geometry on top of the structure that is already present in differential geometry, and is used to define all the other objects we will need. Next, in Sec. 3.2.2 we will use the symplectic form to map smooth functions on the phase space into Hamiltonian vector fields. In Sec. 3.2.3 we will show how the Hamiltonian vector field, corresponding to the Hamiltonian function, can be used to redefine Hamilton's equations within

symplectic geometry. After having redefined Hamilton's equations, in Sec. 3.2.4 we will define the concept of first integrals of motion; smooth functions that are constant on the solutions to the equations of motion. Subsequently, in Sec. 3.2.5 we will define the level sets. Level sets are submanifolds of our phase space, on which the first integrals have specific constant values. Finally, in Sec. 3.2.6 we consider the special case of a system that has N independent first integrals of motion that are in involution. Two integrals are said to be in involution if their Poisson bracket vanishes.

3.2.1 Symplectic form

In the geometric framework of Hamiltonian mechanics, the phase space $\mathcal{M}$ is not only smooth, but also a 2N-dimensional symplectic manifold. A symplectic manifold is a smooth manifold with a global non-degenerate closed 2-form $\mathbf{\Omega}$, called the symplectic form. i.e. $\mathbf{\Omega}(\mathbf{u}, \mathbf{v}) = 0$ for all tangent vectors $\mathbf{v} \in \mathcal{T}_x\mathcal{M}$ if and only if $\mathbf{u}$ is the zero vector, where $\mathcal{T}_x\mathcal{M}$ denotes the tangent space at $x \in \mathcal{M}$ (see Sec. 2.3 for a recap on tangent spaces in differential geometry), and $\mathbf{d\Omega} = 0$, where d denotes the exterior derivative (see Sec. 2.4.5 for a recap on the exterior derivative). On this manifold we define the symplectic coordinates (p_α, q_α) as local coordinates in which the symplectic form becomes [16]:

$$\mathbf{\Omega} = \mathbf{dp}^\alpha \wedge \mathbf{dq}_\alpha. \tag{3.5}$$

3.2.2 Hamiltonian vector fields

The symplectic form links each smooth function H with a unique vector field $\mathbf{X_H}$, called the Hamiltonian vector with Hamiltonian function H, on our symplectic manifold $\mathcal{M}$ in the following way [24]:

$$\imath_{\mathbf{X_H}}\mathbf{\Omega} = \mathbf{\Omega}(\mathbf{X_H}, ...) = \mathbf{dH}, \tag{3.6}$$

where the operation on the left-hand side is the interior product (see Sec. 2.4.6 for a recap of the interior product), and the one form on the right-hand-side is the exterior derivative of the function F. Uniqueness of this vector field follows from the non-degeneracy of the symplectic form.

Hamiltonian vector fields have the property that each diffeomorphism ρ_t generated by them preserves $\mathbf{\Omega}$ (see Sec. 2.3.4 to see how vector fields generate diffeomorphisms). I.e.:

$$\rho_t^*\mathbf{\Omega} = \mathbf{\Omega}, \tag{3.7}$$

where the operation on the left-hand side is the pullback (see Sec. 2.4.2 for a recap of the pullback map). In this way, each smooth function on $\mathcal{M}$ gives rise to a family of symplectomorphisms, which are diffeomorphisms that preserve the symplectic structure. A symplectomorphism corresponds to the physicist's notion of a canonical transformation of the phase space.

3.2.3 Hamilton's equations in symplectic coordinates

In symplectic coordinates (q_α, p_α) the Hamiltonian vector field takes the following form [25]:

$$\mathbf{X_H} = \frac{\partial H}{\partial p_\alpha}\frac{\partial}{\partial q^\alpha} - \frac{\partial H}{\partial q_\alpha}\frac{\partial}{\partial p^\alpha}, \tag{3.8}$$

since we have:

$$\begin{aligned} \imath_{\mathbf{X_H}}\mathbf{\Omega} &= \imath_{\mathbf{X_H}}\mathbf{dq}^\alpha \wedge \mathbf{dp}_\alpha \\ &= \left(\imath_{\mathbf{X_H}}\mathbf{dq}^\alpha\right) \wedge \mathbf{dp}_\alpha - \mathbf{dq}^\alpha \wedge \left(\imath_{\mathbf{X_H}}\mathbf{dp}_\alpha\right) \\ &= \frac{\partial H}{\partial p_\alpha}\mathbf{dp}_\alpha + \frac{\partial H}{\partial q_\alpha}\mathbf{dq}_\alpha = \mathbf{dH}. \end{aligned} \tag{3.9}$$

Looking at Eq. 3.1b, we can rewrite Hamilton's equations in local symplectic coordinates as:

$$\dot{x} = \mathbf{X_H}(x), \quad x \in \mathcal{M}. \tag{3.10}$$

Geometrically, this form of Hamilton's equations means that the solutions of these equations lie on the integral curve of the Hamiltonian vector field (see Sec. 2.3.3 for a recap of integral curves). In other words, the Hamiltonian vector field lies tangent to the physical trajectories, as is depicted in Fig, 3.1

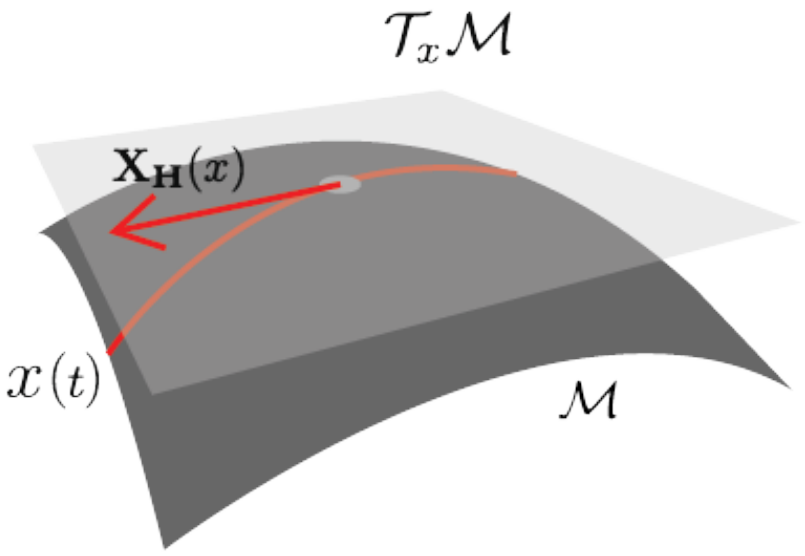

Figure 3.1: The Hamiltonian vector field $\mathbf{X_H}$ lies tangent to the physical trajectories $x(t) \in \mathcal{M}$

3.2.4 First integrals of motion

One of the most useful objects in solving Hamilton's equations are the first integrals of motion P_α. First integrals are smooth functions on $\mathcal{M}$ that are

constant on the solutions to Hamilton's equations [28]. We just showed that the Hamiltonian vector field is tangent to the solutions of Hamilton's equations. Since the first integrals are constant on these solutions, the directional derivative of these first integrals in the direction of the Hamiltonian vector field vanishes.

$$\begin{aligned} 0 &= \mathbf{dP}_\alpha(\mathbf{X_H}) \\ &= \imath_{\mathbf{X_{P_\alpha}}} \mathbf{\Omega}(\mathbf{X_H}) \\ &= \mathbf{\Omega}(\mathbf{X_{P_\alpha}}, \mathbf{X_H}) \\ &= \{P_\alpha, H\}, \end{aligned} \tag{3.11}$$

where $\mathbf{X_{P_\alpha}}$ are Hamiltonian vector fields, defined as in Eq. 3.6, but now with respect to the first integrals P_α. In the last equality, we used the definition of the Poisson bracket in symplectic geometry [29]. Looking back at Eq. 3.3, we note that this definition of the Poisson bracket follows naturally. The Poisson bracket of a function and the Hamiltonian is equal to the total time derivative of this function. The Hamiltonian vector field points in the direction of time evolution by Hamilton's equations. Therefore, it is natural to identify the directional derivative of a function, in the direction of the Hamiltonian vector field, with the Poisson bracket of this function and the Hamiltonian. Furthermore, we identify H with P_1. Clearly, the Hamiltonian itself is a first integral of motion, representing the energy of the system. Some other physical examples of first integrals are linear and angular momentum.

3.2.5 Level sets

We define the level sets $\mathcal{M}_p$ as surfaces where the first integrals have specific constant values $\mathbf{p} = (p_1, \dots, p_N)$:

$$\mathcal{M}_p = \{x \in \mathcal{M} \mid P_\alpha(x) = p_\alpha, 1 \leq \alpha \leq N\}. \tag{3.12}$$

Note that $\mathcal{M}_p$ is a N-dimensional submanifold of $\mathcal{M}$. Following our discussion above, we see that the Hamiltonian vector field $\mathbf{X_H}$ is tangent to the level sets at every point of the level sets, as is also depicted in Fig. 3.2. Furthermore, if a physical trajectory $x(t)$ lies within a level set $\mathcal{M}_p$ at a certain time, it will remain within this level set indefinitely.

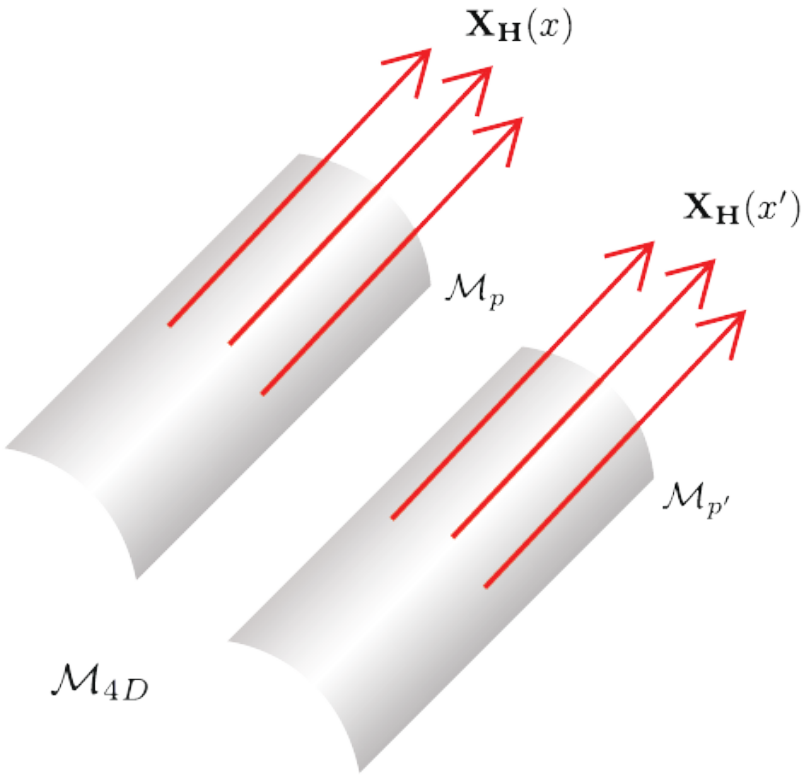

Figure 3.2: Two different 2-dimensional level sets $\mathcal{M}_p$ and $\mathcal{M}_{p'}$ are depicted inside the ambient 4-dimensional phase space. The Hamiltonian vector field $\mathbf{X_H}$ is tangent to the level sets $\mathcal{M}_p$ at all points $x \in \mathcal{M}_p$, and to $\mathcal{M}_{p'}$ at all points $x' \in \mathcal{M}_{p'}$.

3.2.6 N first integrals of motion that are in involution

We are interested in Hamiltonian systems that possess N-independent first integrals of motion P_α. Independent means that they are smooth functions on $\mathcal{M}$ that have linearly independent differentials $\mathbf{dP}_\alpha$. That implies that they form the basis of some cotangent subspace $\subset \mathcal{T}^*_x\mathcal{M}$, and their corresponding Hamiltonian vectors form the basis of some tangent subspace $\subset \mathcal{T}_x\mathcal{M}$. Furthermore, we require the N first integrals to be in involution, which means that the Poisson brackets of all first integrals are identically zero [30]:

$$\{P_\alpha, P_\beta\} = 0 \quad \forall \quad \alpha, \beta \in \{1, \dots, N\}, \tag{3.13}$$

As previously mentioned, the Poison bracket of two first integrals P_α and P_β is equal to the value of the one form $\mathbf{dP}_\alpha$ along the vector Hamiltonian vector field $\mathbf{X_{P_\beta}}$. From this, we conclude that now all Hamiltonian vector fields $\mathbf{X_{P_\alpha}}$ are tangent to the level sets $\mathcal{M}_p$, since all first integrals are in involution and constant on these level sets. I.e., the Hamiltonian vector fields $\mathbf{X_{P_\alpha}}$ form the basis of the tangent space to $\mathcal{M}_p$.

Now we can define completely integrable systems; 2N-dimensional Hamiltonian systems that have some open neighbourhood $\mathcal{U} \subset \mathcal{M}$, for which there exist

N independent first integrals of motion that are in involution for all $x \in \mathcal{U}$, are called completely integrable on the open neighbourhood $\mathcal{U}$ [29]. These systems are foliated by the level sets $\mathcal{M}_p$ i.e., the level sets are N-dimensional leaves that do not intersect, and the phase space is the union of all these leaves.

As alluded to before, the Hamiltonian vector fields $\mathbf{X}_{\mathbf{P}_\alpha}$ form the basis of the tangent space to $\mathcal{M}_p$. This means that each tangent vector of $\mathcal{M}_p$ can be written as a linear combination of these basis vectors, using this and Eq. 3.13, we conclude that the pullback of the symplectic form to $\mathcal{M}_p$ vanishes.

3.3 Action-angle variables

Now that we know what it means for a Hamiltonian system to be completely integrable, we will be able to state the Liouville-Arnold theorem and its consequences. This is a classical theorem that posits the existence of symplectic action-angle coordinates. These local coordinates are ideal to quickly extract the dynamics of a system, and are useful to check for resonances of the system.

First, in Sec. 3.3.1 we will state the Liouville-Arnold theorem and its consequences. Subsequently, in Sec. 3.3.2 we will give a recipe for defining the action variables in a coordinate invariant way. In Sec. 3.3.3 we will show Hamilton's equations in the action-angle variables, this form of the equations is particularly simple. Finally, in Sec. 3.3.4 we will dive into a one-dimensional harmonic oscillator as a toy model, this simple model still shows all the features that we have developed thus far.

3.3.1 The Liouville-Arnold theorem

If a system is completely integrable in some open neighbourhood $\mathcal{V}$ near a level set, and this level set is compact and connected, we can use a classical theorem by Liouville and Arnold. The idea of compactness refers to the set having no punctures or missing endpoints. The theorem states [16]: The level set $\mathcal{M}_p$ is diffeomorphic to an N-torus T^N (see Sec. 2.2.5 for the definition of T^N). Hence, the local coordinates on $\mathcal{M}_p$ are periodic. Furthermore, the open neighbourhood $\mathcal{V}$ is diffeomorphic to the direct product $T^N \times \mathcal{B}$, where $\mathcal{B}$ is an open ball of dimension N, see Fig. 3.3.
There exist symplectic coordinates $(J_\alpha, \varphi_\alpha)$, $1 \leq \alpha \leq N$, called the action-angle variables, on $\mathcal{V}$ ($J_\alpha \in \mathcal{B}, \varphi_\alpha \in T^N$) for which the angle variables φ_α are periodic,

$$\varphi_\alpha + 2\pi = \varphi_\alpha, \tag{3.14}$$

and for which the first integrals depend only on the action variables, $P_\alpha = P_\alpha(J_1, \dots, J_N)$. Note this indeed means that the first integrals have a constant value on the level set $\mathcal{M}_p$, since they don't depend on the local angle coordinates of the level set.

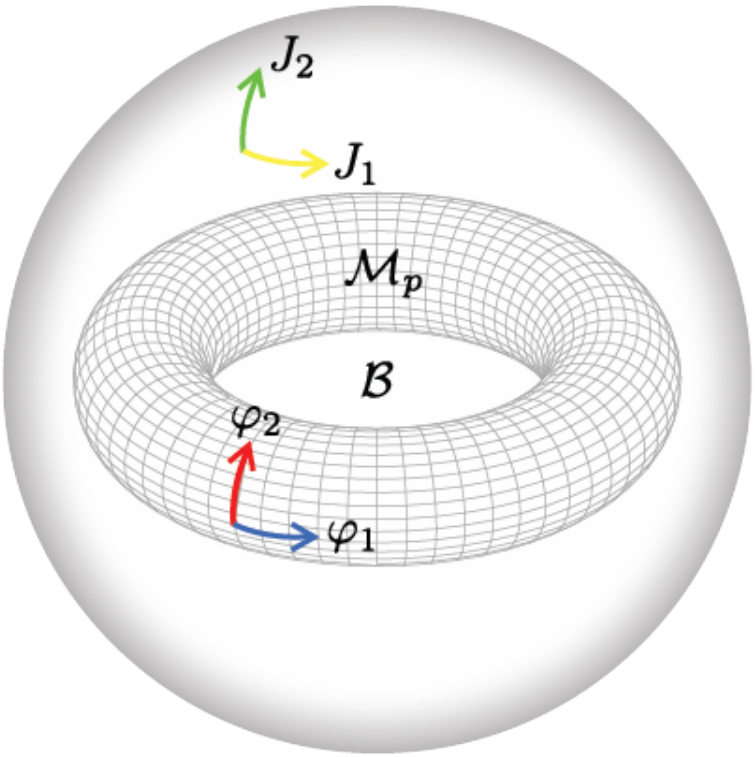

Figure 3.3: The open neighbourhood $\mathcal{V}$, of a 4-dimensional phase space that satisfies the Liouville Arnold theorem, is projected down on a 2-dimensional plane. The action coordinates J_1 and J_2 are local coordinates on the open ball $\mathcal{B}$. The angle coordinates φ_1 and φ_2 are local coordinates on the level set $\mathcal{M}_p$, which is diffeomorphic to a 2-torus.

3.3.2 Coordinate invariant definition of the action variables

In physics, we often make use of specific local coordinates, in order to carry out calculations. It is important that the physical quantities that we calculate, do not depend on the local coordinates that we use, since there is nothing physical about a specific set of local coordinates. Before we provide a coordinate-invariant recipe for defining a set of action variables, we must first define a symplectic potential $\mathbf{\Theta}$. A symplectic potential is a 1-form whose exterior derivative gives the symplectic structure [16], i.e. :

$$\mathbf{d\Theta} = \mathbf{\Omega}. \tag{3.15}$$

Since the symplectic structure is closed, such 1-form potentials always exist locally. If we are for example in the local symplectic coordinates (q_α, p_α), the symplectic potential given by $\mathbf{\Theta} = p^\alpha dq_\alpha$ leads to the correct symplectic form. Note that there is no unique symplectic potential, adding any exact 1-form to

the expression above also works, since the exterior derivative of an exact form vanishes. The same applies to adding a closed 1-form, with exact forms as a subgroup. However, this raises issues regarding the independence of our action variables from the choice of symplectic potential, as we will show below.

The final ingredient we need to make the action variables coordinate independent is the first homotopy group of our level sets $\Pi_1(\mathcal{M}_p)$ (see Sec. 2.1.3 for a definition of $\Pi_1(\mathcal{M}_p)$). Using the Liouville-Arnold theorem, we know that our level sets are diffeomorphic to N-tori. This means that both topological spaces have the same homotopy groups since a diffeomorphism is by necessity also a homeomorphism which preservers topological properties, and the homotopy group of the N-torus is well known: $\Pi_1(\mathcal{M}_p) = \Pi_1(T^N) = Z^N$, the group of integer N-tuples. Each homotopy class is classified by how many times the map that was defined in Sec. 2.1.3 wraps around each of the N unit circles of the torus, hence the first homotopy group is Z^N. Now pick a set of generators of $\Pi_1(\mathcal{M}_p)$: $\{\gamma_1, ..., \gamma_N\}$ (see Sec. 2.1.2 for a recap on group generators). For each generator γ_α, we define the corresponding action variable as:

$$J_\alpha = \frac{1}{2\pi} \oint_{\gamma_\alpha} \boldsymbol{\Theta}. \tag{3.16}$$

Note that this definition is independent of the choice of the symplectic potential. For example, suppose we let $\boldsymbol{\Theta}' = \boldsymbol{\Theta} + df$ for some smooth function f on $\mathcal{M}$. The difference between J_α and J'_α is

$$\frac{1}{2\pi} \int_{\gamma_\alpha} (\boldsymbol{\Theta} - \boldsymbol{\Theta}') = \frac{1}{2\pi} \int_{\gamma_\alpha} df = \frac{1}{2\pi} \int_{\partial\gamma_\alpha} f = 0, \tag{3.17}$$

where in the second to last step we used Stokes' theorem (see Sec. 2.4.7 for a recap of Stokes' theorem), and in the last step we used the fact that the generators are loops and hence do not have a boundary. The trick with Stokes' theorem only works when we add an exact 1-form to the symplectic potential, which is why we limit ourselves to this restriction. We conclude that all symplectic potentials lead to the same action variable.

The definition of the action variables also does not depend on the choice of the generators. Suppose we take 2 different choices γ_α and γ'_α. Now the difference between J_α and J'_α becomes [16]

$$\frac{1}{2\pi} \left(\int_{\gamma_\alpha} - \int_{\gamma'_\alpha} \right) \boldsymbol{\Theta} = \frac{1}{2\pi} \int_{\partial R} \boldsymbol{\Theta} = \frac{1}{2\pi} \int_R \boldsymbol{\Omega} = 0, \tag{3.18}$$

where R is a surface in $\mathcal{M}_p$ which is bounded by $\partial R = \gamma_\alpha - \gamma'_\alpha$, as is shown in Fig. 3.4. In the second to last step we used Stokes' theorem again and in the last step we used that the pullback of Ω to $\mathcal{M}_p$ vanishes.

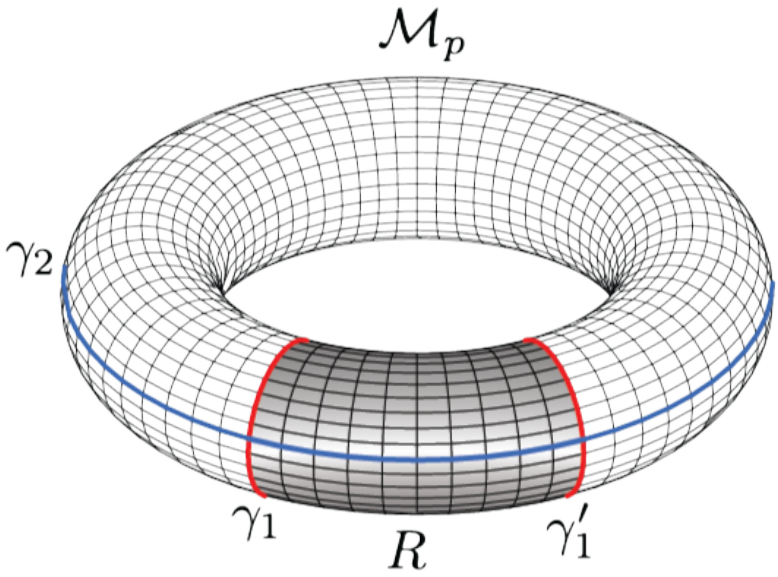

Figure 3.4: Two different choices for generators γ_1 and γ_1', of a two-dimensional level set $\mathcal{M}_p$, and the surface R which they enclose are depicted.

3.3.3 Hamilton's equations in action-angle variables

The Hamiltonian is one of the first integrals, meaning that when we go to the action angle variables, it only depends on the action variables. Hamilton's equations of motion 3.1a now take the following simple form:

$$\dot{J}_\alpha = \frac{\partial H(\mathbf{J})}{\partial \varphi_\alpha} = 0, \tag{3.19a}$$

$$\dot{\varphi}_\alpha = \frac{\partial H(\mathbf{J})}{\partial J_\alpha} = \omega_\alpha, \tag{3.19b}$$

where ω_α are the characteristic frequencies of our system. Note that the action variables are constants of motion. This makes sense since our first integrals are functions of these variables and also constants of motion.

3.3.4 Toy model: one-dimensional harmonic oscillator

Now that we have introduced this elaborate mathematical framework of geometric Hamiltonian mechanics, it is useful to consider a simple toy model to get more familiar with it. Following in the footsteps of most branches of physics, we will start by studying the well known system of a one dimensional harmonic oscillator. The Hamiltonian of this system is given by [26]:

$$H = \frac{p^2}{2m} + \frac{1}{2}m\omega^2 q^2 = E, \quad \omega = \sqrt{\frac{k}{m}}, \tag{3.20}$$

where m is the mass of the particle on the spring, k is the spring's constant, and ω is the angular frequency of the system. Hamilton's equations 3.1a are given by:

$$\dot{q} = \frac{p}{m}, \quad \dot{p} = -m\omega^2 q, \tag{3.21}$$

whose solution is given by [26]:

$$q(t) = \sqrt{\frac{2E}{m\omega^2}} \sin(\omega t + \omega_0), \quad p(t) = \sqrt{2mE} \cos(\omega t + \omega_0), \tag{3.22}$$

where ω_0 depends on the initial conditions of the system. The system has a 2-dimensional phase space, with symplectic coordinates (q, p). The first integral of motion is the Hamiltonian, which gives the energy of the system. The Hamiltonian is in involution with itself, furthermore, our first integrals are automatically linearly independent since we only have one. As a result, the one dimensional harmonic oscillator is integrable on its entire phase space. Note that these arguments hold for any system with a 2-dimensional phase space, they are always completely integrable.

The level sets of this system $\mathcal{M}_E$ are given by the different energies E, E' the system can have. If we look at the solutions of the coordinates in phase space, the different level sets are given by ovals of different sizes. Two different level sets are depicted in Fig. 3.5. These ovals are diffeomorphic to circles, for which it is well known that they are compact. Hence, the level sets are compact and the Liouville-Arnold theorem discussed in Sec. 3.3.1 holds. In fact, circles are 1-Tori, so we see that the level sets are indeed diffeomorphic to 1-Tori.

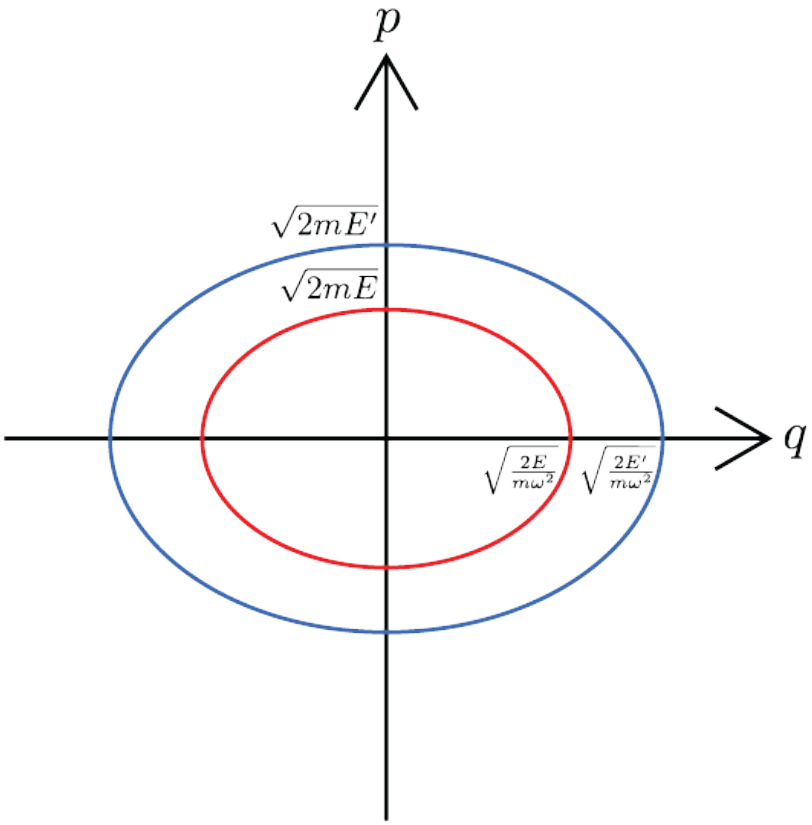

Figure 3.5: Depicted is the 2-dimensional phase space of the harmonic oscillator. Since the system is completely integrable, this phase space is foliated by level sets. For clarity of the picture, only 2 level sets are shown. $\mathcal{M}_E$ is the level set corresponding to a system that has energy E, and $\mathcal{M}_{E'}$ is the level ser corresponding to a system with energy E', where we took $E < E'$.

Next, we will derive a formula for the action variable J_E, by the method described in Sec. 3.3.2. The Homotopy group of the 1-Tori is Z. We will choose the element -1 as its generator to perform the integral, representing counterclockwise integration over the level set in the phase space. Now we need a formula for the symplectic potential (see Eq. 3.15), following [26] we get:

$$\mathbf{\Theta} = pdq = \sqrt{2mE - m^2\omega^2q^2}dq = \frac{2E}{\omega}\cos^2\theta d\theta. \tag{3.23}$$

In the first equality we used the Hamiltonian to get an expression for p in terms of q, and in the final equality we substituted the solution to the equation of motion of q. Now plugging this expression for the symplectic potential into Eq. 3.16 we get:

$$J_1 = \frac{1}{2\pi}\int_{\gamma_1}\mathbf{\Theta} = \frac{E}{\pi\omega}\int_0^{2\pi}\cos^2\theta d\theta = \frac{E}{\omega}. \tag{3.24}$$

We can invert this expression to get a formula for the Hamiltonian in local action-angle variables:

$$E = H = \omega J_1. \tag{3.25}$$

We see that the Hamiltonian indeed becomes a function only depending on the action variable, as stated in the Liouville-Arnold theorem. If we now plug this form of the Hamiltonian in Hamilton's equation's 3.19b, we get a formula for the time derivative of the angle variable.

$$\dot{\varphi_1} = \frac{\partial H}{\partial J_1} = \omega, \tag{3.26}$$

which, as stated in the beginning of this section, is indeed the angular frequency of a linear harmonic oscillator. Using the action-angle variable formulation to acquire this frequency is like craking a walnut with a sledgehammer. Nonetheless, it is a nice check to see that the formalism works. Integrating the previous expression gives us the time dependence of the angle variable:

$$\varphi_1(t) = \omega t + \varphi_0. \tag{3.27}$$

3.4 Marsden Weinstein phase space reduction

Now that we know how to formulate Hamiltonian systems in symplectic geometry, we will delve into a different key concept. When there exists a symmetry group acting symplectically on a Hamiltonian system, the degrees of freedom of the system can be reduced. Marsden and Weinstein first formulated the general procedure of reducing the phase space of such systems [31]. In this section, we will discuss their general procedure.

We start in Sec. 3.4.1, by briefly explaining what it means for a group to act symplectically on a symplectic manifold. Next, in Sec. 3.4.2 we will develop the concept of a moment map. We will also give an interesting aplication of the moment map, reformulating Noether's theorem. Finally, in Sec. 3.4.3 we will state the general theorem that was proven Marsden and Weinstein, and explain how to derive the new Hamiltonian function on the reduced phase space.

3.4.1 Symplectic group action

A group action Ψ is symplectic if the map $\Psi_g = \Psi(g, \cdot)$ is a symplectomorphism for all the group elements g of the group G (see Sec. 2.5.4 for a recap on group actions). This means that the action preserves the symplectic structure, i.e. $\Psi_g^* \mathbf{\Omega} = \mathbf{\Omega}$. Looking at Eq. 3.7, we see that Hamiltonian vector fields generate a symplectic action of the real numbers $\mathbb{R}$ on our symplectic manifold.

3.4.2 Moment maps

Now that we have defined symplectic actions of Lie groups, we can delve into the concept of moment maps of these actions. This concept was first developed by Souriau [32]. Assume we have a symplectic action Ψ of a Lie group G on a symplectic manifold $\mathcal{M}$. Every element ξ of the Lie algebra $\mathfrak{g}$ of G (See Sec. 2.5.1 for a recap on Lie algebras) naturally induces the vector field $\xi_{\mathcal{M}}$ on $\mathcal{TM}$ by Eq. 2.51

A moment map J is a map from the symplectic manifold into the dual of the Lie algebra of G (see Sec. 2.5.2 for a recap on dual Lie algebras).

$$J : \mathcal{M} \to \mathfrak{g}^* \tag{3.28}$$

Which in turn generates a generalized Hamiltonian function J_ξ in the following way [24]:

$$J_\xi(x) = \xi \circ \mathbf{J}(x) = \langle \mathbf{J}(\mathbf{x}), \xi \rangle. \tag{3.29}$$

Geometrically, J_ξ is the component of $\mathbf{J}$ along ξ. J is a moment map for the Lie group G provided that J_ξ is a Hamiltonian function that belongs to the Hamiltonian vector field $\xi_{\mathcal{M}}$ for all the Lie algebra elements $\xi \in \mathfrak{g}$. I.e., looking at Eq. 3.6 we get:

$$\mathbf{d}\mathbf{J}_\xi = \imath_{\xi_{\mathcal{M}}} \mathbf{\Omega}. \tag{3.30}$$

Symplectic actions, for which there exists a moment map that satisfies all the above-mentioned properties, are called Hamiltonian actions.

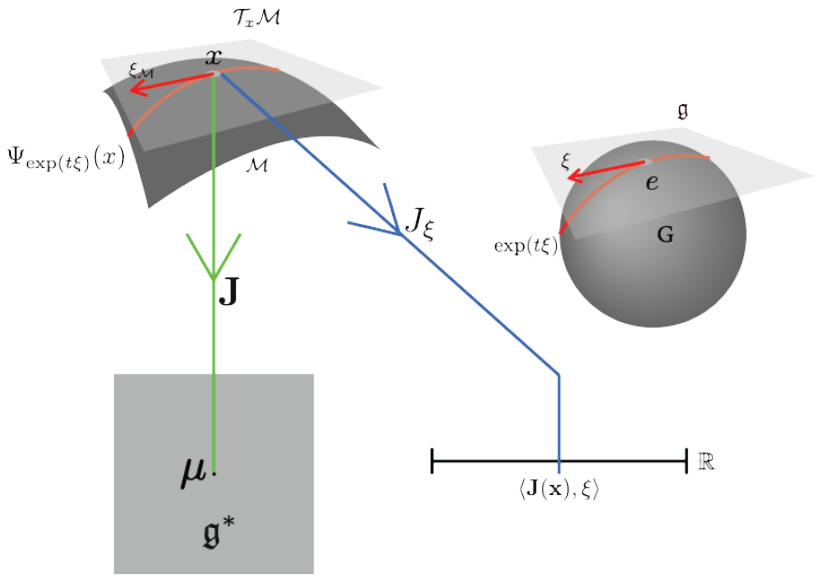

Figure 3.6: The green arrow represents the moment map, which maps a point x of the manifold $\mathcal{M}$ to the dual Lie algebra $\mathfrak{g}^*$. The blue arrow represents the generalized Hamiltonian function J_ξ, which first maps a point x in the manifold $\mathcal{M}$ to the dual Lie algebra, using the green map, and then computes the inner product of this with ξ, an element of the Lie algebra $\mathfrak{g}$, resulting in a real number. All manifolds and their mappings are depicted accordingly.

An interesting application of the moment map is that we can recast Noether's theorem using it [33]. If our Hamiltonian function H is invariant under a Hamiltonian action Ψ, of the Lie group G, i.e. the following equality holds:

$$H(\Psi_g(x)) = H(x), \tag{3.31}$$

for every coordinate $x \in \mathcal{M}$ and every group element $g \in G$. Then the momentum map J of the action Ψ is conserved on every integral curve of the Hamiltonian vector field $\mathbf{H}$. Solutions to Hamilton's equations 3.10 lie on these integral curves, i.e., the Momentum map is a constant of motion and in turn the generalized Hamiltonian function J_ξ is conserved.

If we would for instance look at the Hamiltonian action of three-dimensional displacements, which is given by additions of $\mathbb{R}^3$, the moment map of this action is given by the linear momentum. If we instead look at rotations of our phase space, this is generated by the Hamiltonian action of $SO(3)$ on our phase space. The moment map of this action is given by the angular momentum [24]. If we now apply the above version of Noether's theorem, we get the well known result; that a Hamiltonian system that is invariant under translations has its linear momentum conserved, and a Hamiltonian system that is invariant under rotations has its angular momentum conserved. These two specific examples of moment maps are also the origin of the name of this map, a generalization of the linear and angular momenta.

3.4.3 Marsden Weinstein reduction

By Noether's theorem, if the Hamiltonian function H is invariant under the Hamiltonian group action Ψ, the momentum map J is constant on each integral curve of the Hamiltonian vector field $\mathbf{H}$. From this we conclude that the set $J^{-1}(\mu)$, which is the pullback of a point μ in the dual Lie algebra $\mathfrak{g}^*$, has some interesting properties. If an integral curve of the Hamiltonian vector field $\mathbf{H}$ passes through one point of this set, then this curve is actually entirely contained within the set. If we make the further requirement that μ is a regular value of the momentum map, then by the regular value theorem, $J^{-1}(\mu)$ is a submanifold of our phase space $\mathcal{M}$.

We require that the momentum map J is Ad^*-equivariant, which means that the following equality holds [31]:

$$j(\Psi_g(x)) = Ad^*_{g^{-1}} J(x), \tag{3.32}$$

for every group element $g \in G$, where Ad^* is the co-adjoint action (see Sec. 2.5.5 for a recap on the co-adjoint action). Generally, a Lie group G maps the manifolds $J^{-1}(\mu)$ into each other. However, now that our moment map is Ad^*-equivariant, the isotropy subgroup G_μ of G under the co-adjoint action, i.e., $G_\mu = \{g \in G \mid Ad^*_{g^{-1}}\mu = \mu\}$, leaves $J^{-1}(\mu)$ fixed [30]. The orbit space $J^{-1}(\mu)/G_\mu$, which consists of all unique orbits of G_μ on $J^{-1}(\mu)$, is now well-defined. If we finally require that the group G_μ acts freely and properly on $J^{-1}(\mu)$, meaning that there are no fixed points, then the orbit space becomes a symplectic manifold which we will call the reduced symplectic manifold $\mathcal{M}_\mu = J^{-1}(\mu)/G_\mu$. This reduced symplectic manifold has a unique symplectic structure $\mathbf{\Omega}_\mu$, that satisfies:

$$\pi^*_\mu \mathbf{\Omega}_\mu = i^*_\mu \mathbf{\Omega}, \tag{3.33}$$

where $\pi_\mu : J^{-1}(\mu) \to \mathcal{M}_\mu$ is the canonical projection and $i_\mu : J^{-1}(\mu) \to \mathcal{M}$ is the inclusion. Furthermore, there is a Hamiltonian function H_μ on $\mathcal{M}_\mu$ which satisfies:

$$H_\mu \circ \pi_\mu = H \circ i_\mu, \tag{3.34}$$

this is called the reduced Hamiltonian.

3.5 Resonances

The type of motion we find along our level sets depends on the characteristic frequencies ω_α of our Hamiltonian system. There exist the following resonance conditions for integrable Hamiltonian systems [20]:

$$k_\alpha \omega^\alpha = 0, \quad k_\alpha \in \mathbb{Z} \quad \text{and} \quad |\mathbf{k}| = \sum_\alpha |k_\alpha| \neq 0. \tag{3.35}$$

The number of resonant conditions fulfilled by the motion of our system are equal to the number of linearly independent N-tupples of integers $\mathbf{k}$ we can find,

for which the above condition holds. I.e., resonant tori have rational ratios of frequencies, while non-resonant tori have irrational ratios of frequencies.

When our system satisfies no resonant conditions, the motion will gradually cover our level surface, without passing through the same point twice. This is called a dense quasiperiodic orbit, an orbit that is bounded and confined to a surface but not closed. If, however our system satisfies $m < N - 1$ resonance conditions, the motion will have a dense quasiperiodic orbit over a (N-m)-Torus. If our system satisfies N-1 resonant conditions the motion is periodic.

3.6 Introducing non-integrability

Thus far, we have primarily focussed on Hamiltonian systems that are completely integrable. In Sec. 3.3.1 we demonstrated that for these systems there exist symplectic action-angle coordinates in which the Hamiltonian depends only on the action coordinates: $H(\mathbf{J})$. In such completely integrable systems, we can integrate the equations of motions, leading to analytical solutions. However, as Poincaré's work has long shown, a general dynamical system is non-integrable [34]. These non-integrable systems generally cannot be solved analytically. What is even more detrimental to our predictive power is that chaotic motion often occurs within these systems.

Chaotic motion is defined as follows: if we slightly perturb the initial conditions of our system, the system evolves to a completely different state in phase space, making it extremely sensitive to its precise initial conditions. It is important to note that although chaotic motion is highly sensitive to the initial conditions, it remains deterministic following the equations of motions. Therefore, it qualitatively lies somewhere between the deterministic regular motion of integrable systems and the unpredictable stochastic behavior characterized by complete randomness. [26]

Fortunately, many non-integrable systems can be approximated as integrable systems. By adding a small non-integrable perturbation, we obtain the full system. E.g., the many-body problem is generally non-integrable; however, we can still predict the orbits of the planets around the Sun. The masses of the planets are approximately 0.001 times the mass of the Sun [30], allowing us to approximate the system as the integrable two-body problem of the planet in question and the Sun. To consider the full non-integrable system, we introduce a small perturbation due to the mutual attraction between the planets. The hope is that this small perturbation only slightly deforms the system's motion, and that the qualitative behavior from the integrable approximation still holds. In this section, we will explore when this is the case and when it is not.

The setup is as follows: we start with an integrable Hamiltonian, H_0, such as the two-body system in our previous example. Next, we add a non-integrable component, H_1, representing the mutual attraction of the planets:

$$H(\mathbf{J}, \boldsymbol{\varphi}) = H_0(\mathbf{J}) + \epsilon H_1(\mathbf{J}, \boldsymbol{\varphi}) \tag{3.36}$$

where ϵ is a small perturbation parameter. In the example above, this would correspond to the mass ratio between the planets and the Sun.

3.6.1 The KAM theorem

Many methods of classical perturbation theory for celestial systems have been studied by Poincaré. A fundamental problem with all these methods is that they are plagued by divergent series, rendering them ineffective over infinite time intervals [30]. Significant progress was made by Kolmogorov in 1954 when he sketched a proof for the existence of quasi-periodic motion in nearly integrable Hamiltonian systems [35]. Kolmogorov meticulously detailed the first step, which was his primary contribution, but provided only an outline for the second step, making it a sketch rather than a complete proof. Moser later provided a full proof for certain non-analytic Hamiltonians, where only a finite number of derivatives exist [36]. Arnold focused on the analytic case, as Kolmogorov did, and developed a complete proof that deviated from Kolmogorov's proposed outline for proving convergence [34]. As a result, the theorem became known as the KAM theorem, named after its three main contributors.

We will formulate the KAM theorem similar to Arnold's approach, as we will use it to study an analytical Hamiltonian system. If a completely integrable non-degenerate Hamiltonian system H_0 is perturbed by a sufficiently small conservative perturbation H_1, most non-resonant invariant tori survive and are only slightly deformed. That is, for most initial conditions, the perturbed system again exhibits quasi-periodic motion that densely fills these deformed invariant tori in its phase space [30].

It is important to note that the theorem focuses only on the invariant non-resonant tori, as defined in Sec. 3.5. Near the resonant tori in the unperturbed phase space is where chaotic motion in the perturbed phase space can occur, as we will discuss in the next section. Therefore, a condition can be placed on which invariant tori survive: those that satisfy the Diophantine condition [37]:

$$k_\alpha \omega^\alpha \geq \frac{\gamma}{|\mathbf{k}|^\tau}, \quad \mathbf{k} \in \mathbb{Z}^n, \tag{3.37}$$

for fixed $\tau > n - 1$. The typical choice for γ is $\sqrt{\epsilon}$, where ϵ is the perturbation parameter defined in Eq. 3.36.

The Diophantine condition has a geometric interpretation in the space of frequency vectors $\omega(\mathbf{J})$, which is diffeomorphic to $\mathbb{R}^n$ [37]. As mentioned before, we aim to avoid the resonant tori, which lie in the phase space of our system. To achieve this, we need to pull back the geometry of the Diophantine condition into the phase space of the system. This can be accomplished if the frequency mappings:

$$\omega_i : J^n \to \mathbb{R}^n, \tag{3.38}$$

where J^n denotes the space of all action variables for the system, and we have n different frequencies on each level set $\mathcal{M}_p$ labeled by the index i, satisfies a non-

degeneracy condition [37]. Kolmogorov realized that if the frequency mappings are functionally independent, which is the case if the following condition holds:

$$\det\left(\frac{\partial\omega}{\partial\mathbf{J}}\right) = \det\left(\frac{\partial^2 H_0}{\partial\mathbf{J}^2}\right) \neq 0, \tag{3.39}$$

then this can be achieved. This condition actually makes the frequency mappings a local diffeomorphism, allowing us to indeed pull back the geometry of the Diophantine condition [37]. If our system satisfies this condition, it is called non-degenerate. Arnold proved that it is sufficient if the ratio of frequency vectors is functionally independent on each constant energy shell of H_0 [34]. This mathematically translates to the following condition:

$$\det\begin{pmatrix} \frac{\partial\omega}{\partial\mathbf{J}} & \omega \\ \omega & 0 \end{pmatrix} = \det\begin{pmatrix} \frac{\partial^2 H_0}{\partial\mathbf{J}^2} & \frac{\partial H_0}{\partial\mathbf{J}} \\ \frac{\partial H_0}{\partial\mathbf{J}} & 0 \end{pmatrix} \neq 0. \tag{3.40}$$

If this condition is satisfied by the system on each energy level set, it is called iso-energetic non-degenerate.

The KAM theorem actually has two slightly different outcomes, depending on whether it is applied to a non-degenerate system, or a iso-energetic non-degenerate system. In the former case, the frequency vectors of the deformed tori remain the same as for the unperturbed system, while in the latter case, the frequency vectors might change, but the frequency ratios remain the same. Furthermore, in an iso-energetic non-degenerate system, the deformed torus resides at the same energy (the value of H) as the unperturbed torus (the value of H_0) [29].

Chapter 4

Modified gravity

Now that we have developed the mathematical framework to study general dynamical systems, we will take a brief detour to introduce the modified gravity theories under analysis. We will begin by further motivating the need for modified gravity, followed by an introduction to the specific theories. This will lay the groundwork for developing the model used to study EMRIs within these frameworks.

General Relativity , introduced by Einstein in 1915, is a cornerstone of modern physics. It describes spacetime as a dynamical entity curved by energy densities. Throughout this chapter, we assume a working knowledge of GR. As a reminder, the Einstein-Hilbert action in geometric units ($c = G = 1$) is given by [38]:

$$S_{EH} = \frac{1}{16\pi} \int \sqrt{-g} R d^4x, \tag{4.1}$$

where R is the Ricci scalar, a number that summarizes the curvature of a manifold. In GR, this manifold is typically the spacetime under study. The vacuum field equations of GR are derived by minimizing this action with respect to the metric, which leads to:

$$G_{\mu\nu} = R_{\mu\nu} - \frac{1}{2} R g_{\mu\nu} = 0, \tag{4.2}$$

where $G_{\mu\nu}$ is the Einstein tensor, $R_{\mu\nu}$ the Ricci tensor, and $g_{\mu\nu}$ the metric tensor. Taking the trace of this equation demonstrates that $R = 0$ for vacuum solutions, consistent with the absence of matter-induced curvature. This further reduces the vacuum field equations:

$$R_{\mu\nu} = 0. \tag{4.3}$$

The GR field equations accurately describe most large-scale gravitational phenomena. For example, they explain the precession of Mercury's perihelion, a phenomenon unaccounted for by Newtonian mechanics. GR also predicts gravitational lensing, the bending of light by massive objects, and has enabled precise

calculations of time dilation experienced by satellites, crucial for GPS functionality. Furthermore, GR's predictions were spectacularly confirmed by the first direct observation of gravitational waves [11], and shortly afterward, the first image of a black hole, Sagittarius A*, the supermassive black hole at the center of our galaxy, was captured [39].

Given this huge empirical success of GR [2], one may start to wonder why would we want to modify this theory? Despite its succes in describing solar system-scale physics, GR encounters profound challenges in certain regimes. In classical GR, singularities, points in spacetime where both the curvature and the density become infinite, are unavoidable in some solutions, such as black holes and the Big Bang [40]. These infinities are physically puzzling, and it is widely believed that quantum effects should smooth out such singularities [41].

Attempts to quantize GR, particularly through the standard covariant quantization approach of quantum field theory (QFT), face formidable challenges. In renormalizable QFTs like the Standard Model, divergences in calculations can be canceled by adding a finite number of counterterms. However, applying this approach to GR reveals that an infinite number of counterterms are required to handle divergences, making GR non-renormalizable. Non-renormalizable theories, while often considered problematic, can still be used as effective field theories that provide valid predictions up to a certain energy scale [5].

For example, the Schrödinger equation, central to early quantum mechanics, describes a non-renormalizable system. Nevertheless, it makes accurate predictions at energies below the electron mass. Its UV completion, the Dirac equation and quantum electrodynamics, is a renormalizable theory [3]. Similarly, GR as an effective field theory works well at low energies, but a UV completion is required to extend its validity to high energies.

Two prominent candidates for the UV completion of quantum gravity are string theory and loop quantum gravity. The problem is that the energy scale at which new gravitational physics is believed to come into play is far beyond our experimental capabilities of detection. This has made these UV completions of quantum gravity speculative thus far. Any UV-complete theory of gravity must recover GR in the appropriate low-energy limit, a criterion met by both string theory and loop quantum gravity. For more details, see [8, 10].

One way to address the non-renormalizability problem is by adding quadratic curvature terms to the action, which have been shown to render the theory renormalizable [19]. However, as Ostrogradsky first proved [42], such higher-derivative terms in the action or equations of motion lead to ghost instabilities in the theory. A ghost is a state with negative energy or norm, meaning that an infinite number of positive- and negative-energy particles can be produced at zero energy cost, which is not physically viable. However, there exist specific combinations of higher-curvature terms in the action where all higher-order derivatives in the equations of motion cancel out. This chapter explores two such extensions: in Sec.4.1, we examine scalar Gauss-Bonnet (sGB) gravity, and in Sec.4.2, we discuss dynamical Chern-Simons (dCS) gravity.

4.1 scalar Gauss-Bonnet gravity

sGB theories extend the Einstein-Hilbert action by incorporating a real, massless scalar field coupled to a quadratic curvature term [43]:

$$S_{sGB} = \frac{1}{16\pi}\int \sqrt{-g}\left(R + \alpha_{GB} f(\varphi)\mathcal{G} - \frac{1}{2}\left(\nabla\varphi\right)^2\right)d^4x, \tag{4.4}$$

where α_{GB} is the Gauss-Bonnet coupling constant and ∇ is the covariant derivative. $\mathcal{G}$ is called the Gauss-Bonnet invariant, which is given by:

$$\mathcal{G} = R^2 - 4R_{\mu\nu}R^{\mu\nu} + R_{\mu\nu\alpha\beta}R^{\mu\nu\alpha\beta}, \tag{4.5}$$

where $R^{\mu\nu\alpha\beta}$ is the Riemann tensor. This specific combination of quadratic curvature terms cancels all higher-order derivatives beyond second order in the metric field equations [18], thereby avoiding Ostrogradsky instabilities. Furthermore, the Gauss-Bonnet invariant can be expressed as the divergence of a vector field [44]. This implies that if only the Gauss-Bonnet invariant appears in the action, we could apply Stokes' theorem to convert it into a boundary term, which is typically neglected and does not affect the theory. Therefore, a scalar field must be coupled to the Gauss-Bonnet term, rather than just a constant.

Many forms of coupling functions $f(\varphi)$ have been studied in the literature. A noteworthy subclass are theories where the coupling function is exponential in the scalar field, these can be derived as a low energy limit after compactification to 4 dimensions in heterotic string theory [9]. Such theories are termed Einstein-Dilaton-Gauss-Bonnet gravity, where the scalar field corresponds to the dilaton field.

For the rest of this thesis we will focus on the simplest coupling function, just a linear one, leading to the following action:

$$S_{sGB} = \frac{1}{16\pi}\int \sqrt{-g}\left(R + \alpha_{GB}\varphi\mathcal{G} - \frac{1}{2}\left(\nabla\varphi\right)^2\right)d^4x. \tag{4.6}$$

this theory is often referred to as shift symmetric sGB gravity, since this action is invariant under constant shifts of the metric [45]. For the kinetic term of the scalar field this is easy to see. The coupling term has this symmetry since the Gauss-Bonnet invariant can actually be written as the divergence of a vector field. Therefore, the constant shift only introduces a boundary term, which can be disgarded in most cases [44].

We find the following modified Gauss-Bonnet field equations by minimizing the action with respect to the metric tensor [46]:

$$G_{\mu\nu} = \frac{1}{2}\nabla_\mu\varphi\nabla_\nu\varphi - \frac{1}{4}g_{\mu\nu}\left(\nabla\varphi\right)^2 - 4\alpha_{GB}P^{\beta}_{\mu\alpha\nu}\nabla^\alpha\nabla_\beta\varphi, \tag{4.7}$$

where $P^{\beta}_{\mu\alpha\nu}$ represents the divergence-free part of the Riemann tensor and can be written as:

$$P^{\beta}_{\mu\alpha\nu} = g_{\mu\lambda}\delta^{\lambda\beta\sigma\delta}_{\nu\rho\gamma\rho}R^{\gamma\rho}_{\sigma\delta}, \tag{4.8}$$

with δ the generalized Kronecker delta symbol. plugging this back into our field equations, we find:

$$G_{\mu\nu} = \frac{1}{2}\nabla_\mu\varphi\nabla_\nu\varphi - \frac{1}{4}g_{\mu\nu}\big(\nabla\varphi\big)^2 - 4\alpha_{GB}g_{\mu\lambda}\delta^{\lambda\beta\sigma\delta}_{\nu\rho\gamma\rho}R^{\gamma\rho}_{\sigma\delta}\nabla^\alpha\nabla_\beta\varphi. \tag{4.9}$$

Similarly, if we minimize the action with respect to the scalar field we find the scalar field equation:

$$\Box\varphi = -\alpha_{GB}\mathcal{G}, \tag{4.10}$$

where $\Box = \nabla_\mu\nabla^\mu$ is the covariant D'Alembertian. This is a Klein-Gordon equation sourced by the Gauss-Bonnet invariant.

4.2 dynamical Chern-Simons gravity

We just observed that the Gauss-Bonnet invariant avoids Ostrogradsky instabilities because all higher-order derivatives beyond second order in the metric equations of motion cancel. Another combination of quadratic curvature terms that achieves the same result [47] is the Pontryagin density ${}^*RR$, which is defined as:

$${}^*RR = {}^*R^{\mu\nu\alpha\beta}R_{\mu\nu\alpha\beta} = \frac{1}{2}\epsilon^{\mu\nu\gamma\delta}R^{\alpha\beta}_{\gamma\delta}R_{\mu\nu\alpha\beta}, \tag{4.11}$$

where ${}^*R^{\mu\nu\alpha\beta}$ the dual Riemann tensor, and $\epsilon^{\mu\nu\alpha\beta}$ the Levi-Civita tensor. The Pontryagin density can also be expressed as as the divergence of a vector field [17]:

$${}^*RR = \nabla_\mu K^\mu = \nabla_\mu\epsilon^{\mu\alpha\beta\delta}\Gamma^\nu_{\alpha\gamma}\left(\partial_\beta\Gamma^\gamma_{\delta\nu} + \frac{2}{3}\Gamma^\gamma_{\beta\sigma}\Gamma^\sigma_{\delta\nu}\right), \tag{4.12}$$

where $\Gamma^\mu_{\alpha\beta}$ is the Christoffel symbol.This implies that the Pontryagin density must be coupled to a function of spacetime; otherwise, it reduces to a vanishing boundary term. However, there is an important distinction from the Gauss-Bonnet invariant. Due to the presence of the Levi-Civita tensor in the Pontryagin density, it is a pseudo-scalar, meaning it is parity-odd [17]. To preserve parity symmetry at the level of the action, the Pontryagin density must be coupled to a pseudo-scalar field rather than a scalar field.

Jackiw and Pi first introduced non-dynamical Chern-Simons gravity [48], the action that describes the theory in geometric units reads:

$$S_{CS} = \frac{1}{16\pi}\int\sqrt{-g}\left(R + \frac{\alpha_{CS}}{4}\vartheta\,{}^*RR\right)d^4x. \tag{4.13}$$

where α_{CS} is the Chern-Simons coupling constant.

Smith et al. [49] introduced a canonical kinetic term for the scalar field ϑ, rendering it dynamical. This theory is described by the following action:

$$S_{dCS} = \frac{1}{16\pi}\int\sqrt{-g}\left(R + \frac{\alpha_{CS}}{4}\vartheta\,{}^*RR - \frac{1}{2}\big(\nabla\vartheta\big)^2\right)d^4x. \tag{4.14}$$

If we minimize this action with respect to the metric tensor, we find the following modified field equations [17]:

$$G_{\mu\nu} = \frac{1}{2}\nabla_\mu\vartheta\nabla_\nu\vartheta - \frac{1}{4}g_{\mu\nu}\big(\nabla\vartheta\big)^2 - \alpha_{CS}C_{\mu\nu}, \tag{4.15}$$

where $C_{\mu\nu}$ is referred to in the literature as the Cotton-York tensor, it is given by:

$$C^{\mu\nu} = \nabla_\alpha\vartheta\epsilon^{\alpha\beta\delta(\mu}\nabla_\delta R^{\nu)}_\beta + \nabla_\alpha\nabla_\beta\vartheta^* R^{\beta(\mu\nu)\alpha}, \tag{4.16}$$

where the round brackets around the indices means the symmetrization of the tensor in these indices. If we minimize the action with respect to the scalar field ϑ, we again find a Klein-Gordon equation, but this time sourced by the Pontryagin density:

$$\Box\vartheta = -\frac{\alpha_{CS}}{4}{}^*RR. \tag{4.17}$$

Chapter 5

Conserved quantities in time-like geodesics around a black hole and the effective potential

An extreme mass ratio inspiral (EMRI) consists of a supermassive black hole ($10^4 M_\odot \leq M \leq 10^7 M_\odot$) and a stellar-mass compact object, such as a black hole, a neutron star, or something more exotic. During the final year before the stellar-mass compact object plunges into the supermassive black hole, the system undergoes approximately 10^4–10^5 orbits. These orbits occur very close to the event horizon of the supermassive black hole, within its strong-curvature regime [50]. The large number of orbits in LISA's sensitivity range allows small deviations from General Relativity to accumulate, and the strong-field nature of these orbits makes EMRIs an ideal laboratory for testing potential deviations from General Relativity. While current uncertainties in EMRI astrophysics make it difficult to predict how many EMRIs LISA will detect, even the most pessimistic models suggest that EMRIs will be a likely source for LISA.

This chapter outlines the modeling framework for EMRI systems under the approximation that the small object can be treated as a test particle. Additionally, the gravitational radiation reaction of EMRIs occurs on a timescale much longer than the orbital motion. As a result, most of the inspiral can be described by the stellar-mass compact object traveling along time-like bound geodesics of the supermassive black hole, transitioning between these geodesics every few orbits as gravitational radiation causes the loss of energy and angular momentum. In Sec. 5.1, we describe the theoretical model of a point particle traveling along bound geodesic orbits of the supermassive black hole. Sec. 5.2 introduces the conserved quantities of this model, which are subsequently used in Sec. 5.3 to establish an effective potential framework.

5.1 The EMRI model

An EMRI system is not completely integrable as a Hamiltonian system, such as is described in Sec. 3.2.6. I.e., the Liouville-Arnold theorem does not hold. As outlined in Sec. 3.6, a useful approach is to approximate the non-integrable system with a closely related integrable one. Given the extreme mass ratio $\frac{\mu}{M} \sim \mathcal{O}(10^{-5})$, with μ the mass of the stellar mass object and M the mass of the supermasive black hole, the supermassive black hole will have a larger impact on the spacetime of the system. As an approximation, we thus take the spacetime to be that of a black hole vacuum solution to Einstein's field equations, as was first done by Ryan [51]. In Sec. 5.1.1 we will introduce the model in General Relativity, after which we add the modified gravity metric perturbations in Sec. 5.1.2.

5.1.1 General Relativity

The no-hair theorem in General Relativity states that black holes are fully characterized by their mass, spin, and electric charge [38]. It is suspected that most astrophysical black holes have spin, since objects with angular momentum fall into them and the angular momentum of the full system is conserved. It is also suspected that most black holes are neutrally charged, since any excess charge density would quickly be neutralized. The vacuum solution to Einstein's field equations for a spinning black hole is the Kerr metric, expressed in Boyer-Lindquist coordinates as [38]:

$$\begin{aligned} ds^2 = g_{\mu\nu}dx^\mu dx^\nu = &-\left(1-\frac{2Mr}{\Sigma}\right)dt^2 - \frac{4Mar\sin^2\theta}{\Sigma}dt\,d\phi \\ &+\frac{\Sigma}{\Delta}dr^2 + \Sigma\,d\theta^2 + \left(r^2+a^2+\frac{2Ma^2r\sin^2\theta}{\Sigma}\right)\sin^2\theta\,d\phi^2, \end{aligned} \tag{5.1}$$

where

$$\Delta = r^2 - 2Mr + a^2, \quad \Sigma = r^2 + a^2\cos^2\theta, \tag{5.2}$$

and a is the angular momentum per mass, which is often referred to as the spin of the black hole, $a = \frac{J}{M}$.

As a first approximation, we will describe the stellar mass object as a point particle with mass μ on a bound geodesic orbit in this spacetime. This system is described by the following Hamiltonian function [52]:

$$\begin{aligned} H = \frac{1}{2}g^{\mu\nu}p_\mu p_\nu = &-\frac{(r^2+a^2)^2 - \Delta a^2\sin^2\theta}{2\Delta\Sigma}p_t^2 - \frac{2aMr}{\Delta\Sigma}p_t p_\phi \\ &+\frac{\Delta - a^2\sin^2\theta}{2\Delta\Sigma\sin^2\theta}p_\phi^2 + \frac{\Delta}{2\Sigma}p_r^2 + \frac{1}{2\Sigma}p_\theta^2 \end{aligned} \tag{5.3}$$

This is a completely integrable system, meaning it has 4 integrals of motion, referred to as conserved quantities in this chapter. We will examine these conserved

quantities in Sec. 5.2. The phase space of this system is eight-dimensional, consisting of four spacetime dimensions and their conjugate momenta. The evolution parameter in this system is the proper time along the geodesics. Proper time represents the time measured by a clock moving along the geodesic, accounting for all time dilation effects caused by spacetime curvature or the relative velocities traveled along the geodesic.

5.1.2 Modified gravity

Building on the work of Cano and Ruipérez, we incorporate the leading-order corrections to the Kerr metric in modified gravity [53]. Their starting point was a metric that is a vacuum solution in GR and zero valued scalar fields. They applied the scalar field equations 4.10 & 4.17 to the background metric to compute the first-order corrections to the scalar fields, appearing at $\mathcal{O}(\alpha)$. Consecutively, they used the modified field equations 4.9 & 4.15, to the background metric and the first correction to the scalar field, to calculate the first order correction of the metric, appearing at $\mathcal{O}(\alpha^2)$.

As the background metric $g^{(0)}_{\mu\nu}$, they used the Kerr metric 5.1. For the metric corrections $g^{(1)}_{\mu\nu}$, they employed a general ansatz that respects the symmetries of a Kerr-like spacetime: stationarity, meaning the spacetime geometry does not change with time, and axisymmetry, meaning the spacetime is symmetric about the axis of rotation. The ansatz they adopted was:

$$\begin{aligned} ds^{(1)2} =& H_1 dt^2 - H_2 \frac{4Mar(1-x^2)}{\Sigma} dt d\phi + H_3 \Sigma \left(\frac{dr^2}{\Delta} + \frac{dx^2}{1-x^2} \right) \\ &+ H_4 \left(r^2 + a^2 + \frac{2Ma^2 r(1-x^2)}{\Sigma} \right) (1-x^2) d\phi^2, \end{aligned} \tag{5.4}$$

where $x = \cos\theta$. Introducing the dimensionless spin parameter $\chi = \frac{a}{M}$, they performed a power series expansion of the H_i functions and the scalar fields, solving the field equations order by order. They gave solutions to these equations up to order χ^{14}, which are accurate solutions for $\chi < 0.7$ (where $\chi = 1$ is the extreme value of a Kerr black hole where it becomes unstable [38].)

The system now still describes a point particle on a bound geodesic orbit, but this time in the space time of a Kerr black hole in our 2 modified gravity theories. The Hamiltonian is given by:

$$H = \frac{1}{2} \left(g^{\mu\nu}_{(0)} + g^{\mu\nu}_{(1)} \right) p_\mu p_\nu, \tag{5.5}$$

where $g^{\mu\nu}_{(0)}$ is the inverse of the Kerr metric and $g^{\mu\nu}_{(1)}$ is the inverse of the correction, including the H_i from [53]. This is our setup to study an EMRI system in modified theories of gravity.

There are some shortcomings in our setup. In reality, the smaller compact object perturbs the spacetime, influencing its own dynamics through the additional curvature it generates. This effect is typically modeled as a gravitational

self-force acting on the compact object, a topic that lies beyond the scope of this thesis. For a general overview, see [54], and for an application to an EMRI in General Relativity, see [55]. Additionally, the inspiraling compact object emits gravitational waves, leading to a loss of energy and angular momentum, which causes the orbit to shrink over time. Finally, supermassive black holes reside at the centers of galaxies, where significant amounts of surrounding matter, beyond the inspiraling compact object, may give rise to additional effects such as dynamical friction or tidal perturbations.

5.2 Conserved quantities

Conserved quantities are quantities of a dynamical system that remain constant over time. In Chapter 3, we referred to these as first integrals. As previously discussed in Sec. 3.2.4, every Hamiltonian system has the Hamiltonian itself as a first integral. In this case, the Hamiltonian is proportional to the rest mass of the stellar-mass compact object:

$$H = -\frac{1}{2}\mu^2. \tag{5.6}$$

From Eq. 3.3, the total time derivative of any quantity that is not explicitly time-dependent is given by:

$$\begin{aligned}\frac{\mathrm{d}F}{\mathrm{d}\tau} &= \{F, H\} \\ &= \frac{\partial F}{\partial q_\mu}\frac{\partial H}{\partial p^\mu} - \frac{\partial F}{\partial p_\mu}\frac{\partial H}{\partial q^\mu},\end{aligned} \tag{5.7}$$

where τ is the proper time and the summation convention is applied to μ. Referring to the Kerr Hamiltonian in General Relativity 5.3, we observe that it does not depend on t or ϕ. Consequently, the momenta in the t- and ϕ-directions of the stellar-mass compact object are conserved. These are identified as the energy and angular momentum of the compact object, respectively:

$$p_t = -E, \quad p_\phi = L_z, \tag{5.8}$$

where the negative sign in for energy follows the convention commonly used in the literature.

In the previous section, we noted that a point particle in the Kerr spacetime forms a completely integrable Hamiltonian system. In a four-dimensional spacetime, corresponding to an eight-dimensional phase space, this implies the existence of four conserved quantities. The fourth conserved quantity, known as the Carter constant Q, arises from a hidden symmetry of Kerr spacetime represented by a killing thensor. Furthermore, it ensures the separability of the radial and polar equations of motion. The Carter constant is expressed as [16]:

$$Q = p_\theta^2 + a^2\cos^2\theta\left(\mu^2 - p_t^2\right) + \cot^2\theta p_\phi^2 \tag{5.9}$$

The modified gravity systems are no longer completely integrable. While the same isometries of the metric ensure the conservation of energy and angular momentum, and the Hamiltonian remains a conserved quantity, the Carter constant is absent. In fact, it has been proven that no fourth conserved quantity exists in these systems [56]. This absence implies that the system is not completely integrable, and the Liouville-Arnold theorem discussed in Sec. 3.3.1 does not apply. Furthermore, we expect chaotic motion to occur on resonant orbits around the central black hole.

5.3 The effective potential framework

In this section, we use the conserved quantities derived in the previous section to reduce the geodesic motion in four-dimensional spacetime to a 2-degree-of-freedom system with an effective potential [21]. This reduction makes it easier to analyze key features of the system. In particular, we will use it to identify the regions of physically bound geodesic orbits within the phase space in the next chapter. First, we construct this framework within the context of General Relativity in Sec. 5.3.1. Then, in Sec. 5.3.2, we extend the framework to include the modified gravity metric perturbations introduced earlier in this chapter.

5.3.1 General Relativity

The Hamiltonian (Eq. 5.3) is separated into two components: one depending on the conserved momenta and the other on the non-conserved momenta.

$$H = \frac{1}{2} g^{\mu\nu} p_\mu p_\nu = \frac{1}{2}\left(g^{AB} p_A p_B + g^{CD} p_C p_D \right), \tag{5.10}$$

where $A, B \in \{t, \phi\}$ and $C, D \in \{r, \theta\}$. This separation is possible because the metric contains no cross-terms between these sets of degrees of freedom, i.e., $g^{tr} = g^{t\theta} = g^{\phi r} = g^{\phi\theta} = 0$. We then use the Hamiltonian constant, Eq. 5.6, to further constrain the system:

$$G - \mu^2 = g^{rr} p_r^2 + g^{\theta\theta} p_\theta^2, \tag{5.11}$$

where the summation over C and D has been expanded, and the function G is introduced as:

$$G = -g^{AB} p_A p_B = -g^{tt} E^2 + 2 g^{t\phi} E L_z - g^{\phi\phi} L_z^2. \tag{5.12}$$

Referring again to the Kerr Hamiltonian (Eq. 5.3), we observe that $g^{rr} = \Delta g^{\theta\theta}$. defining $J = g^{\theta\theta}$, we rewrite Eq. 5.11 as:

$$V_{eff} = \frac{1}{J}\left(G - \mu^2\right) = \Delta p_r^2 + p_\theta^2. \tag{5.13}$$

Finally, we will divide everything by the rest mass squared of the stellar mass object, effectively normalizing our energy and angular momentum to $\tilde{E} = \frac{E}{\mu}$

and $\tilde{L_z} = \frac{L_z}{\mu}$. For simplicity, these quantities will be denoted without tildes for the remainder of this thesis. Additionally, the right-hand side of the effective potential now depends on velocities instead of momenta:

$$V_{eff} = \Delta \dot{r}^2 + \dot{\theta}^2, \tag{5.14}$$

where $\dot{x^\mu} = \frac{\mathrm{d}x^\mu}{\mathrm{d}\tau}$, with τ the proper time. It is worth noting that there are various ways to define an effective potential, but all approaches yield identical dynamics because the underlying system remains the same [20].

The effective potential V_{eff} depends on the Kerr metric elements, which are functions of r and θ, as well as the spin of the supermassive black hole, and the energy and angular momentum of the compact object. Thus, given χ, E, and L_z, the effective potential becomes a function of r and θ: $V_{eff}(r, \theta)$. Importantly, V_{eff} is proportional to squared velocities, which are always non-negative. In the Kerr spacetime, the function Δ has a special significance. The event horizon, the boundary beyond which nothing can escape the black hole, is located where $\Delta = 0$. Outside the event horizon Δ is strictly positive, while inside, the coordinate system breaks down. This means that for physical geodesic motion, the effective potential must be non-negative. The curve defined by $V_{eff} = 0$ is referred to as the curve of zero velocity, as it corresponds to geodesics with zero radial and polar velocities [20].

5.3.2 Modified gravity

Now that we have constructed the effective potential framework for the Hamiltonian system that describes geodesics around a Kerr black hole, we extend this framework to the modified gravity system. The Hamiltonian for this system is given by Eq. 5.5, which remains proportional to a contraction of two conjugate momentum vectors by the inverse metric. However, the metric is now given by the Kerr metric, Eq. 5.1, plus a metric perturbation, Eq. 5.4, rather than the Kerr metric alone. Notably, the metric perturbation does not introduce cross terms between the conserved and non-conserved momentum degrees of freedom, allowing us to separate the Hamiltonian again. The Hamiltonian constant remains conserved for the modified gravity theories. using this property and defining G in a manner similar to before, we again obtain:

$$G - \mu^2 = g^{rr} p_r^2 + g^{\theta\theta} p_\theta^2. \tag{5.15}$$

We emphasize that these inverse metric components are now a sum of the inverse Kerr and the inverse perturbed metric components, i.e., $g^{rr} = g^{rr}_{(0)} + g^{rr}_{(1)}$. In our discussion of General Relativity, we observed that $g^{rr}_{(0)} = \Delta g^{\theta\theta}_{(0)}$. We now note that this relationship holds for the metric perturbation, Eq. 5.4, when converting x to θ. This implies that the same relation for the inverse modified gravity metric components: $g^{rr} = \Delta g^{\theta\theta}$. Consequently, we define the effective potential analogously to our earlier approach:

$$V_{eff} = \frac{1}{J}\big(G - 1\big) = \Delta\dot{r}^2 + \dot{\theta}^2. \tag{5.16}$$

In General Relativity, the event horizon of the Kerr black hole is located in the area where $\Delta = 0$. Cano and Ruipérez have shown that this remains true for all modifications to gravity that they considered [53], including sGB and dCS gravity. However, they found that the region where $\Delta = 0$, i.e., the event horizon, is smaller in these modified gravity theories.

The effective potential still depends on the Kerr metric elements, but now also on the metric perturbation elements, which, in turn, depend on the functions H_i. These functions vary with the radial coordinate, the polar coordinate, and the spin of the supermassive black hole. Thus, given χ, E, and L_z, the effective potential remains a function of r and θ. Since Δ is strictly non-negative outside the event horizon, we obtain the same result: the positive region of the effective potential corresponds to the location of physical geodesic orbits around the supermassive black hole. Furthermore, the curve defined by $V_{eff} = 0$ continues to represent the curve of zero velocity, delineating geodesics with zero radial and polar velocities.

Chapter 6

Analysis of the region of geodesic bound orbits

Let us examine a three-dimensional plot of $V_{eff}(r, \theta)$ to understand its structure.

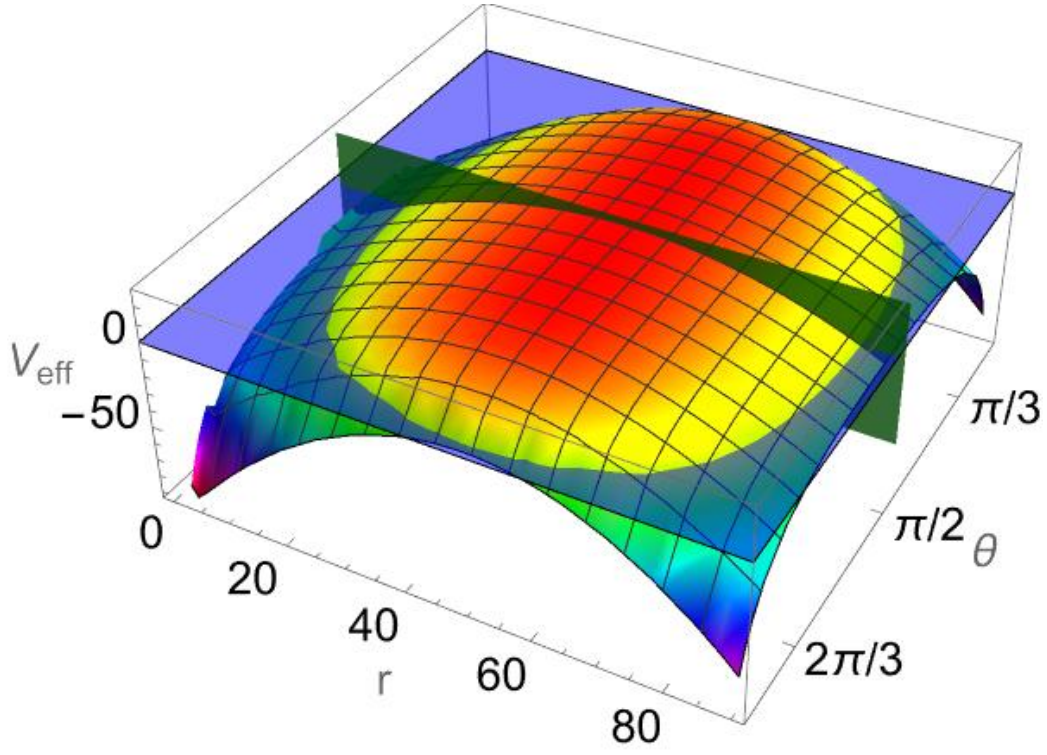

Figure 6.1: The effective potential V_{eff} in Kerr spacetime, with $E = 0.99$, $L_z = 5$, and $\chi = 0.4$, is shown. The plane where $V_{eff} = 0$ is depicted in blue, and the equatorial plane ($\theta = \frac{\pi}{2}$) is shown in green.

It is important to note that from this point onward we have set the mass of the central black hole to $M = 1$, which is equivalent to rescaling distances as $r \to \frac{r}{M}$. In Fig. 6.1, we observe an island where the effective potential is positive.

Its boundary corresponds to the curve of zero velocity at the intersection of the blue plane with V_{eff}. As mentioned in the previous chapter, physical geodesics exist only in regions where the effective potential is non-negative.

From this, we conclude that in a spacetime of a Kerr black hole with a dimensionless spin of $\chi = 0.4$, a particle with an energy per rest mass of 0.99 and an angular momentum per rest mass of 5 enters a bound orbit around the central black hole. It doesn't plunge into the black hole because the effective potential becomes negative before it reaches the event horizon, making the geodesic motion stuck inside the positive island. In astrophysical EMRI systems, the stellar mass object would emit gravitational waves, which in turn drains its energy and angular momentum until it reaches a point where the effective potential allows for a plunge orbit. This is, however, outside the scope of our work. We focus solely on bound geodesic orbits.

It is notable in Fig. 6.1 that the positive island extends both closest to and farthest from the black hole in the equatorial plane, located at $\theta = \frac{\pi}{2}$ and depicted in green. From this observation, we conclude that the roots of the effective potential in the equatorial plane can be used to classify geodesic orbits. For a plunge orbit, $V_{\text{eff}}(r, \frac{\pi}{2})$ has an outer root but no inner root. A bound orbit is characterized by both an outer and an inner root. Finally, a hyperbolic orbit, one in which the object approaches the black hole and then escapes back to infinity,is defined by an inner root but no outer root of the potential in the equatorial plane.

6.1 Bound orbits in General Relativity

To better understand the locations of bound orbits, we will explore the parameter space of the Hamiltonian system. We will analyze and find the roots of the effective potential in the equatorial plane for various values of the supermassive black hole spin χ, the point particle's energy E, and angular momentum L_z.

We found that if the energy per rest mass E is greater than or equal to 1, the orbit is hyperbolic. If E is smaller than 0.99, the location of the outer roots does not change significantly. Therefore, we decided to focus on the region where $E \in [0.99, 0.999]$. Furthermore, we varied $L_z \in [-5, 5]$ to obtain a good overview of the trends in bound orbits and varied χ between 0 and 0.7, as the metric perturbation for modified gravity is only accurate for these spins.

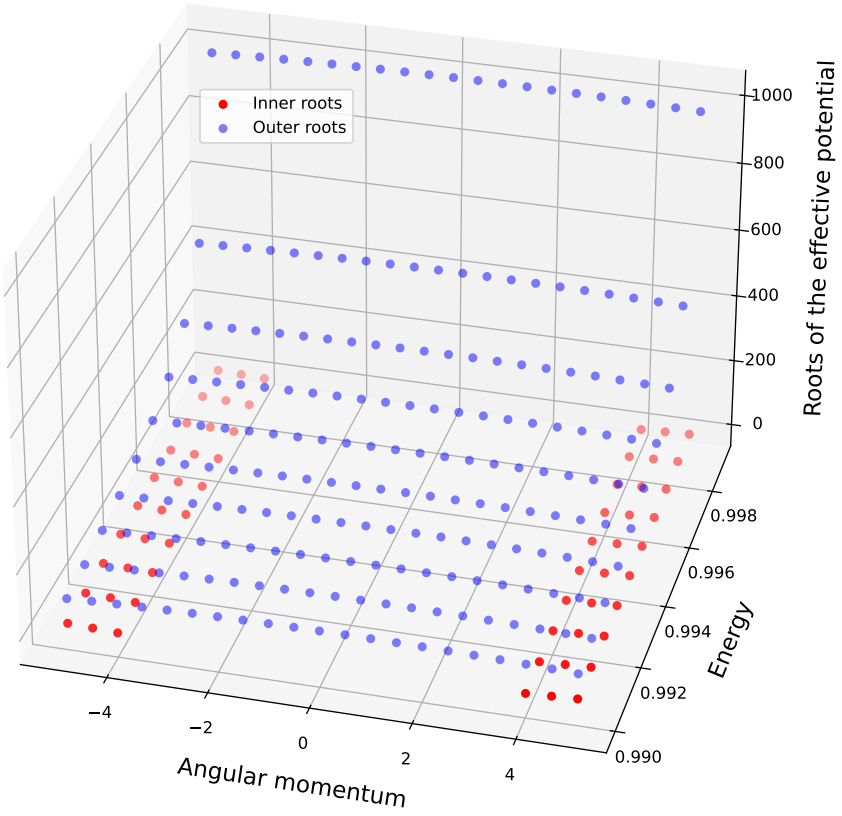

(a) $\chi = 0$

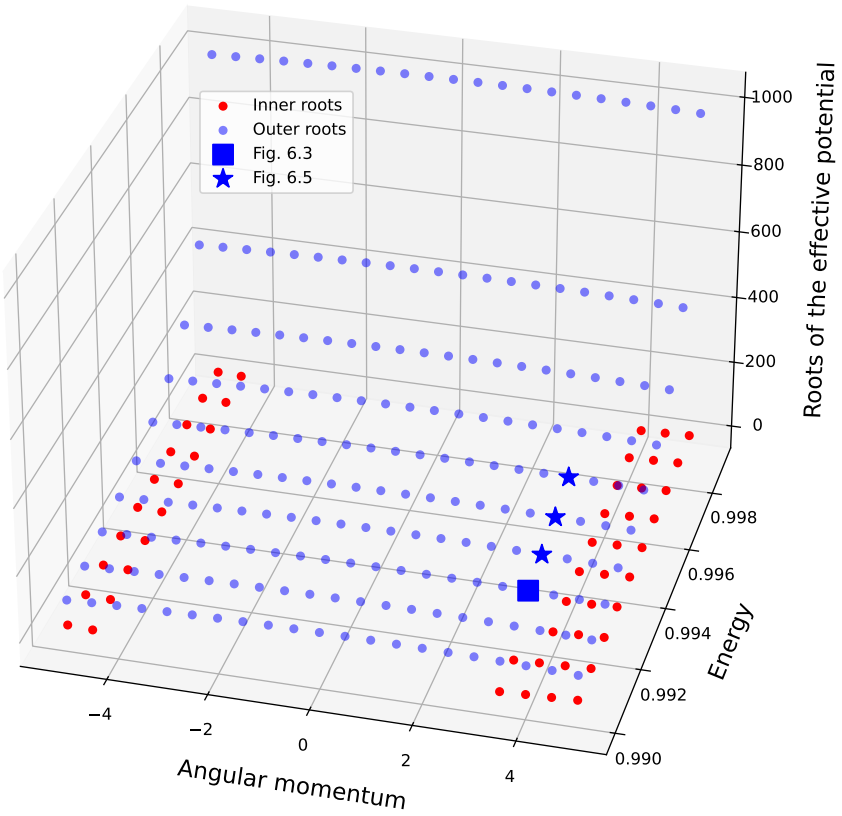

(b) $\chi = 0.4$

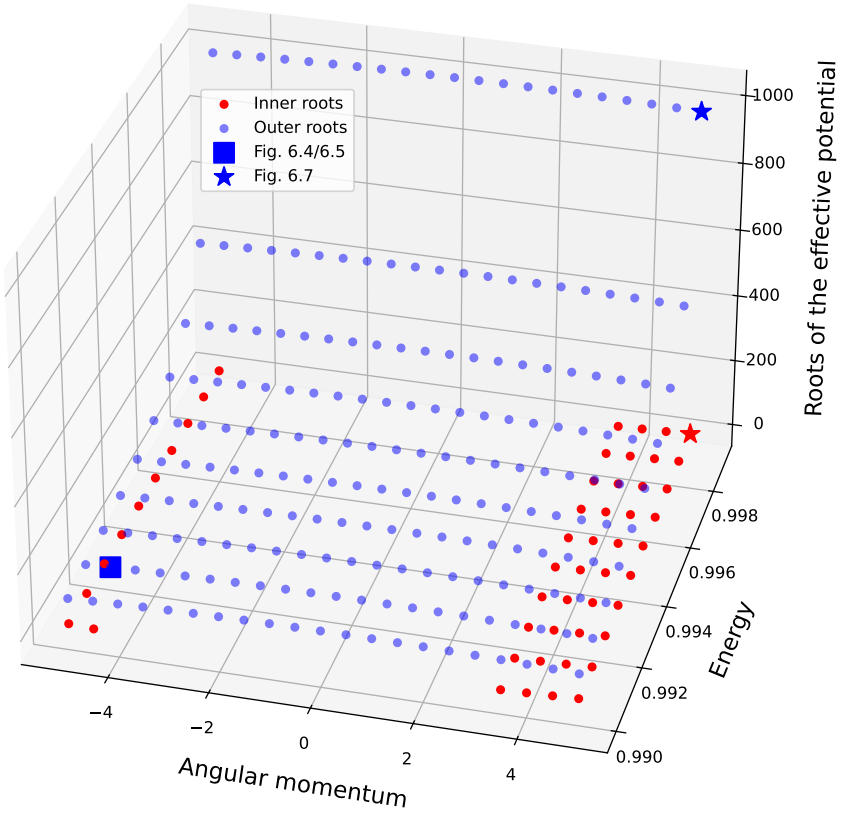

(c) $\chi = 0.7$

Figure 6.1: The roots of the effective potential in the equatorial plane for different values of normalized energy and angular momentum of the infalling compact object. The red dots represent the inner roots, and the blue dots represent the outer roots. (a) Shows a Schwarzschild supermassive black hole without spin, (b) shows a Kerr black hole with a dimensionless spin of $\chi = 0.4$, and (c) shows a Kerr black hole with a dimensionless spin of $\chi = 0.7$. Some dots have been replaced by stars or squares, these are effective potentials that we analyze further in later figures in this chapter, see the legends for the corresponding figures.

We observe two types of orbits in Fig. 6.1. The plunge orbits are located in the center of the figure, where the absolute value of L_z is small, and they have only an outer root. The bound orbits are located to the sides, where the absolute value of angular momentum is larger, and they have both outer and inner roots. This is expected since a compact object requires a minimum amount of angular momentum to orbit a supermassive black hole. Additionally, we observe that as the energy increases, the location of the outer roots moves further away from the supermassive black hole.

One aspect we have not yet discussed is the frame-dragging effect in General Relativity, where the rotation of massive objects "drags" the spacetime around them. This phenomenon is known as the dragging of inertial frames. The mass

of a Kerr black hole is so extreme and concentrated that frame-dragging becomes especially pronounced. Outside the event horizon, there is even a region called the ergosphere, where frame-dragging is so intense that all objects must move in the direction of the black hole's rotation [38]

Inspirals with positive angular momentum move in the same direction as the black hole's spin, which is called a prograde orbit. Those with negative angular momentum move in the opposite direction, referred to as a retrograde orbit. Prograde orbits align with the frame-dragging effect, which reduces the angular momentum required for a bound orbit. Conversely, retrograde orbits oppose the frame-dragging, requiring more angular momentum for a bound orbit. This is exactly what we find in our parameter space sweep.

Fig. 6.1a shows the roots of the effective potential in a black hole without spin, where the Kerr metric reduces to a Schwarzschild metric. We observe that there are the same amounts of inner roots with positive as negative angular momenta, i.e., there are the same amounts of prograde as retrograde bound orbits. This is to be suspected, since there is no frame-dragging effect for Schwarzschild black holes. Fig. 6.1b shows the roots of the effective potential for a black hole with a dimensionless spin of $\chi = 0.4$. Here, we observe the frame-dragging effect: 10 bound retrograde orbits have disappeared, and 2 additional bound prograde orbits have appeared in the sample we are considering. When the dimensionless spin is increased to $\chi = 0.7$, we see in Fig. 6.1c that another 9 retrograde bound orbits have disappeared, and 8 prograde bound orbits have appeared.

In Fig. 6.2, we further analyze the frame-dragging effect by plotting the fraction of bound orbits for both prograde and retrograde orbits as a function of the dimensionless spin χ. Here, we normalize the fraction of bound by the total number of prograde/retrograde orbits, which in our case is 100 for both. We chose to plot the fractions rather than the total number of bound orbits because the fractions are less sensitive to the resolution of the phase space sweep. For a Schwarzschild black hole with no spin, both prograde and retrograde fractions of bound orbits are 0.3. The fraction of prograde orbits peaks at 0.4 for $\chi = 0.5$ and onwards, while the fraction of retrograde orbits decreases to 0.12 at a dimensionless spin of $\chi = 0.7$.

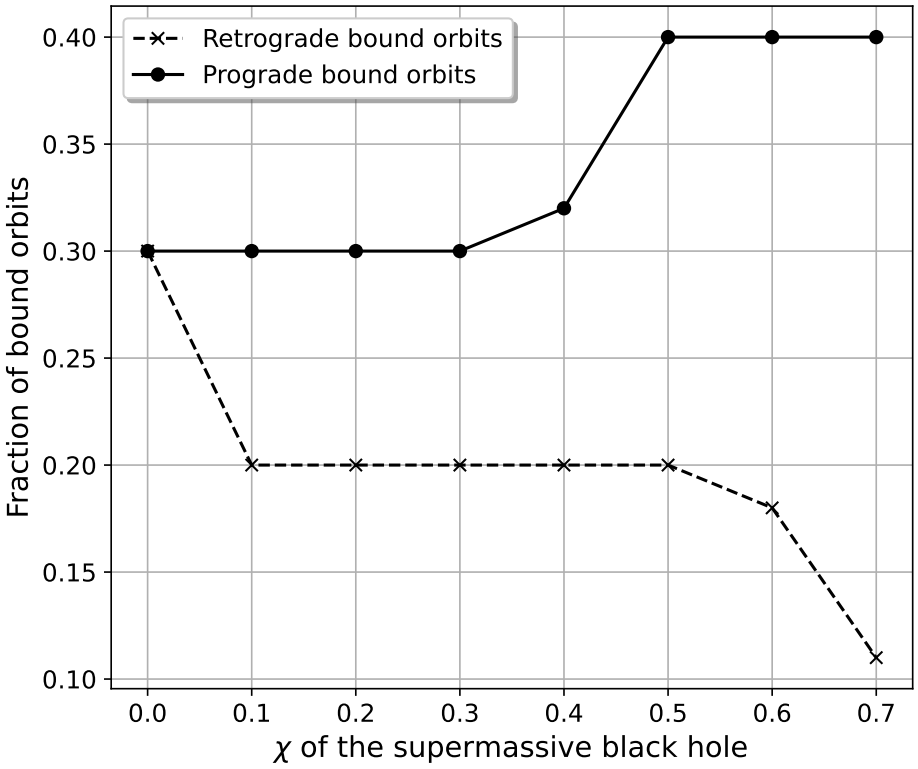

Figure 6.2: The fractions of bound prograde orbits (solid black line) and bound retrograde orbits (dashed black line), each normalized by the total number of prograde and retrograde orbits sampled, respectively, are plotted as functions of the spin of the supermassive black hole

6.2 Bound orbits in modified gravity

Having investigated the region of bound orbits in General Relativity, we now explore how the effective potential behaves when we turn on the coupling constants α_{sGB} and α_{dCS}. First, we set both coupling constants to 0.1. In dCS gravity, we find that the fraction of bound orbits remains similar to that of General Relativity (Fig. 6.2). However, in sGB gravity, we observe a slight change in the fractions. Specifically, for an effective potential with $\chi = 0.4$, $E = 0.992$, and $L_z = 3.5$, corresponding to the square in Fig. 6.1b, an inner root appears when we set $\alpha_{sGB} = 0.1$. This effective potential is shown in Fig. 6.3, where Fig. 6.3a depicts the General Relativity case, and Fig. 6.3b shows the sGB case.

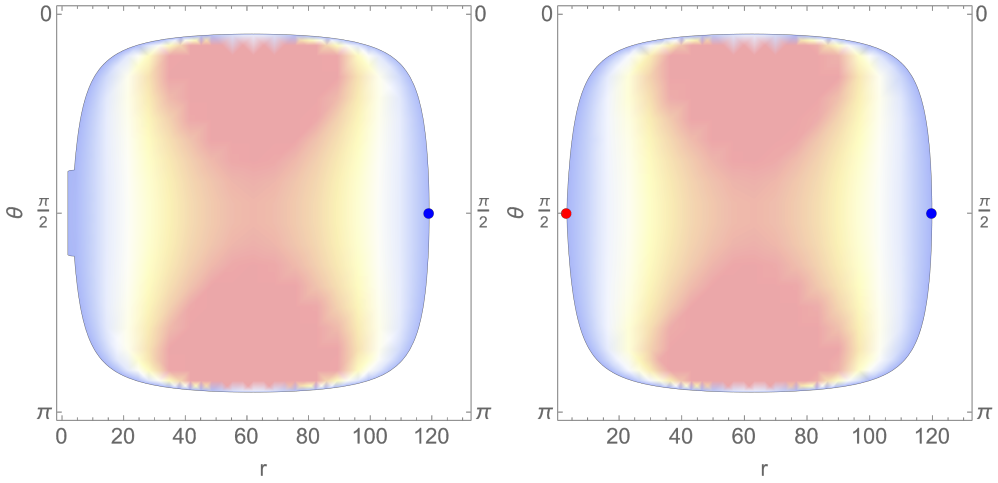

(a) General Relativity **(b)** scalar Gauss-Bonnet

Figure 6.3: The region where the effective potential is positive is plotted as a heatmap, with the roots of the effective potential on the equatorial plane marked. The red dot indicates the inner root, and the blue dot indicates the outer root. (a) corresponds to the square in Fig. 6.1b, and (b) shows the potential in sGB gravity, also with $\chi = 0.4$, $E = 0.992$, $L_z = 3.5$, and additionally with $\alpha_{sGB} = 0.1$.

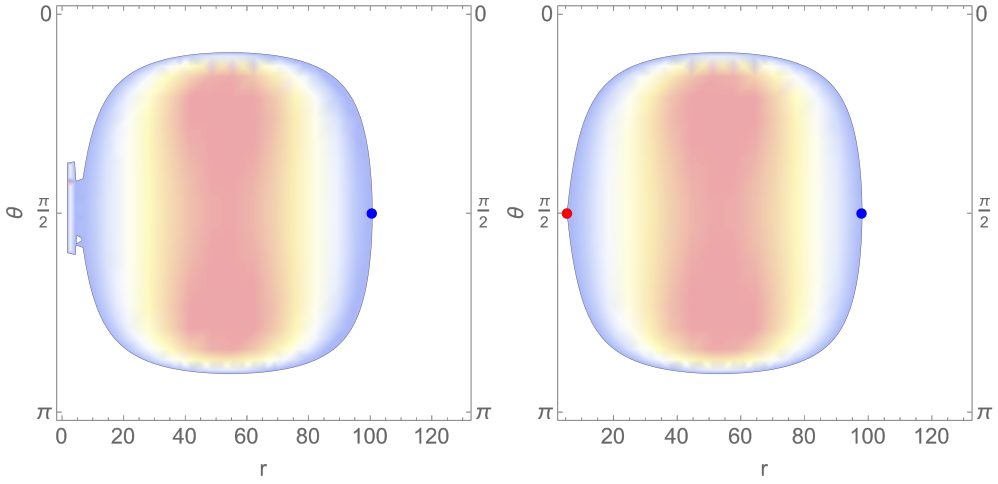

(a) General Relativity **(b)** dynamical Chern-Simons

Figure 6.4: (a) corresponds to the square in Fig. 6.1c, and (b) shows the effective potential in dCS gravity, also with $\chi = 0.7$, $E = 0.991$, and $L_z = -4.5$, with additionally $\alpha_{dCS} = 0.2$.

When we increase the coupling constants to 0.2, dCS gravity exhibits the appearance of an additional bound orbit. For an effective potential with $\chi = 0.7$, $E = 0.991$, and $L_z = -4.5$, corresponding to the square in Fig. 6.1c, an inner root appears when we set $\alpha_{dCS} = 0.2$. This effective potential is shown in Fig. 6.4, with Fig. 6.4a representing the potential in General Relativity and Fig. 6.4b in dCS gravity.

For sGB gravity, when the coupling constant is increased to 0.2, four additional bound orbits emerge, these are illustrated in Fig. 6.5. Fig. 6.5a is related to the same General Relativity potential as the square in Fig. 6.1c. In figures 6.5b-6.5d, we show the effective potentials related to the stars in Fig. 6.1b.

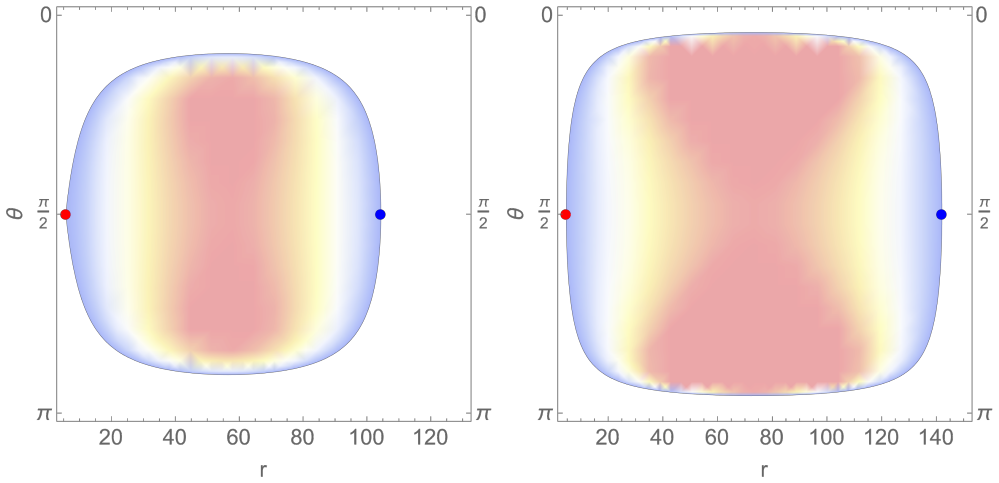

(a) Square in Fig. 6.1c.

(b) Star in Fig. 6.1b (E=0.993).

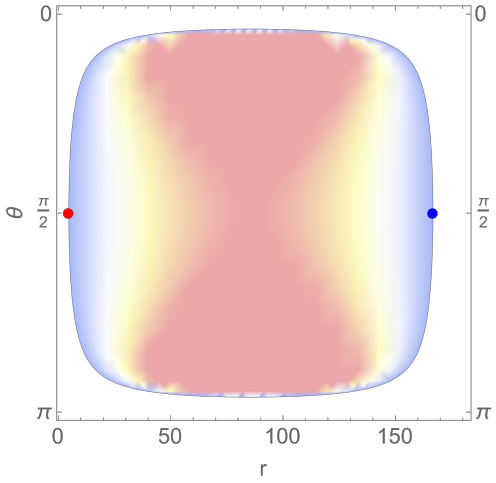

(c) Star in Fig. 6.1b (E=0.994).

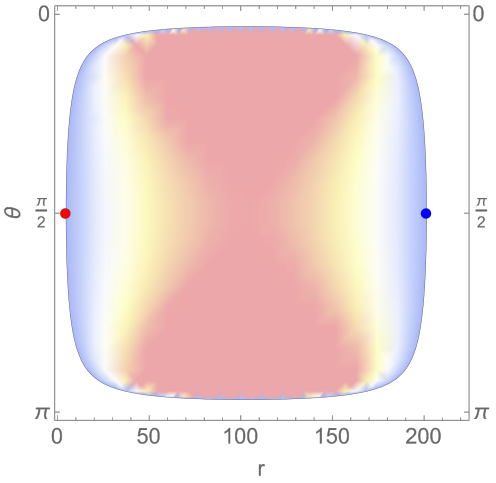

(d) Star in Fig. 6.1b (E=0.995).

Figure 6.5: Four effective potential plots of bound orbits in scalar Gauss-Bonnet gravity, with $\alpha_{sGB} = 0.2$, the related General Relativity effective potentials where plunge orbits and are referred to in the subfigures captions.

To summarize, sGB gravity picks up one additional prograde bound orbit as the coupling constants increase to 0.1. When the coupling constants are increased to 0.2, dCS gravity gains an additional retrograde bound orbit, while sGB gravity gains the same retrograde bound orbits, along with three additional prograde bound orbits. This suggests a trend in both modified gravity theories: they each have a mechanism that reduces the required angular momentum for retrograde bound orbits. Furthermore, sGB gravity reduces the angular momentum requirement for prograde bound orbits as well.

In Fig. 6.6, we examine whether this trend persists at higher coupling constants. We study the fraction of bound orbits for both modified gravity theories in the case of a supermassive black hole with a dimensionless spin of $\chi = 0.7$. The sGB results are shown in green, while the dCS results are shown in yellow. Solid lines represent prograde bound orbits, and dashed lines represent retrograde bound orbits. The results confirm the trend: dCS gravity shows the greatest reduction in required angular momentum for retrograde bound orbits, with no reduction for prograde orbits, while sGB gravity reduces the angular momentum for both prograde and retrograde orbits, with a greater reduction for prograde orbits.

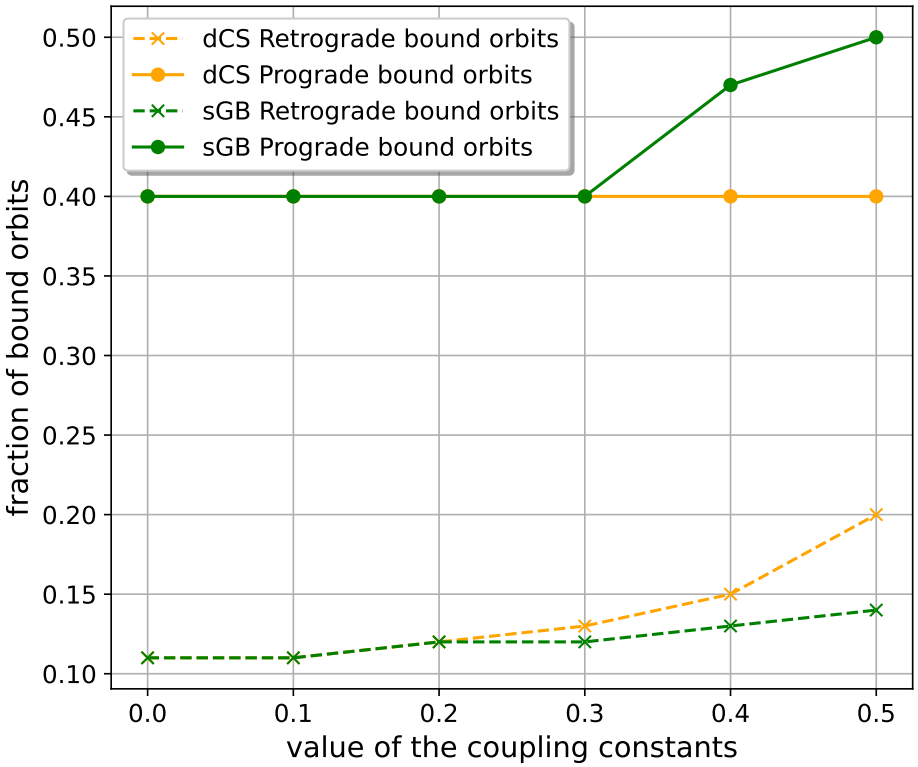

Figure 6.6: The fraction of bound orbits are plotted against the value of the coupling constant for a supermassive black hole with dimensionless spin $\chi = 0.7$. The solid lines correspond to prograde bound orbits, while the dashed lines correspond to retrograde bound orbits. In both cases, green corresponds to sGB gravity and yellow to dCS gravity.

Finally, we observe an intriguing effect: the roots of the effective potential appear to shift inward for dCS gravity and outward for sGB gravity. To illustrate this, in Fig. 6.7 we analyze the roots of the effective potential corresponding to the General Relativity case of the star in Fig. 6.1c. In Fig. 6.7a, we show how the

inner roots of this effective potential change with varying coupling constants, while in Fig. 6.7b, we examine how the outer roots change.

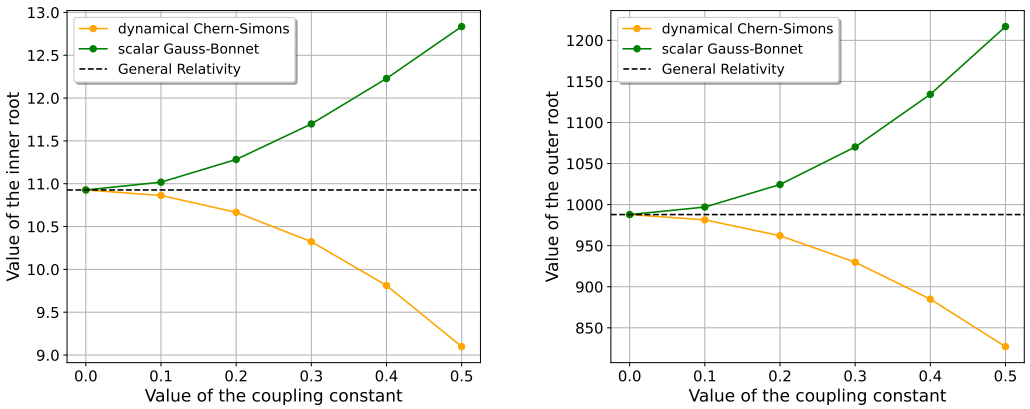

(a) Inner roots **(b)** Outer roots

Figure 6.7: The inner roots in (a) and the outer roots in (b) are plotted against the coupling constants of the modified gravity theories. The green line corresponds to sGB gravity, and the yellow to dCS gravity. The black striped line indicates the roots for General Relativity, corresponding to the star in Fig. 6.1c.

Chapter 7

Discussion and conclusions

We began by developing a general mathematical framework for studying dynamical systems within the paradigm of symplectic geometry, an approach particularly well-suited for analyzing extreme mass ratio inspiral (EMRI) systems. These systems provide an excellent testing ground for probing potential modifications to General Relativity through the analysis of the gravitational waves they emit. To achieve this, a deeper understanding of EMRI dynamics in modified gravity theories is essential, and this framework offers a potential tool for such studies. We combined various tools tailored for such studies, emphasizing the behavior of integrable systems and the effects of non-integrable perturbations, including chaotic motion in resonant orbits. A significant contribution of this work is the explicit development of the Marsden-Weinstein phase space reduction, a concept often implicitly applied in the study of Kerr spacetimes due to their symmetries [52, 15, 55].

After developing the mathematical framework, we introduced the two modified gravity theories studied in this work: sGB and dCS gravity. These theories have been shown to be normalizable as quantum field theories [19], and they arise naturally as low-energy limits of string theory and loop quantum gravity [8, 10]. Using these theories, we constructed a Hamiltonian model to approximate the EMRI as a point particle system, focusing on time-like geodesic bound orbits in the modified gravity spacetimes. These approximations form the basis of EMRI dynamics, and due to the high dimensionality of the parameter space, identifying these bound orbit regions already requires a considerable analysis. Perturbed metrics for these spacetimes were obtained from previous works [53], and we identified conserved quantities to establish an effective potential formalism from first principles, which has proved useful in other contexts in previous works [21]. This effective potential was invaluable for mapping the allowed regions for physical geodesics within the system's parameter space.

In General Relativity, the effective potential accurately predicts the frame-dragging effects of spinning bodies. For instance, as the spin of the central black hole increases, the angular momentum required for prograde bound orbits decreases due to frame-dragging, while the angular momentum required for retrograde bound orbits increases. These trends were previously demonstrated for

circular orbits in [57] using a different effective potential formalism, and for more general orbits in [52] using the action-angle variable formalism. Additionally, the effective potential shows that the region of bound orbits expands farther from the central black hole as the energy of the orbiting body increases, which follows physical intuition.

Turning on the coupling constants α_{sGB} and α_{dCS} allowed us to study the impact of modified gravity on bound orbits. In dCS gravity, for a central black hole with a dimensionless spin of $\chi = 0.7$, the fraction of retrograde bound orbits nearly doubled, increasing from 0.11 to 0.2. In sGB gravity, this fraction increased modestly from 0.11 to 0.15. Interestingly, sGB gravity also increased the fraction of prograde bound orbits from 0.4 to 0.5, whereas dCS gravity did not significantly affect prograde orbits.

It is important to note that the exact fractions of bound orbits depend on the resolution of our phase space sweep. For example, reducing the interval in the angular momentum dimension from 0.5 to 0.25 would yield slightly different fractions. Similarly, extending the cutoff point of $|L_z| \leq 5$ would artificially increase these fractions by adding bound orbits. However, we expect the overall trends, such as the shift of bound regions to lower angular momentum, to remain robust.

Modified gravity theories also altered the position of the effective potential's positive islands, i.e., the region of physical geodesic orbits. In sGB gravity, both inner and outer roots shifted outward, which could place geodesics farther from the central black hole compared to General Relativity. Conversely, in dCS gravity, roots shifted inward, suggesting geodesics closer to the black hole than in General Relativity.

Another important consistency check is to compare our results to the most stringent constraints on the coupling constants of the modified gravity theories. Gravitational wave observations have constrained sGB gravity to $\sqrt{\alpha_{sGB}} < 1.7\,\mathrm{km}$ in S.I. units [58], equivalent to $\sqrt{\alpha_{sGB}} < 1.32 M_\odot$ in geometric units. Similarly, multimessenger neutron star observations have constrained dCS gravity to $\sqrt{\alpha_{dCS}} < 8.5\,\mathrm{km}$ in S.I. units [59], equivalent to $\sqrt{\alpha_{dCS}} < 33.12 M_\odot$ in geometric units. These constraints can be expressed in dimensionless form by dividing by the characteristic length scale of the system, such as the mass of Sagittarius A* ($\approx 4 \times 10^6 M_\odot$ [60]), the supermassive black hole at the center of our galaxy. This yields $\alpha_{sGB} < 1.09 \times 10^{-13}$ and $\alpha_{dCS} < 8.28 \times 10^{-6}$. At these coupling constant values, shifts in geodesic bound orbits do not manifest within the system. However, the primary objective of this study was to provide a proof of concept, demonstrating trends in the changes of geodesic bound orbits under modified gravity theories.

Our work provides a detailed view of how the regions of bound geodesic orbits shift around a Kerr-like black hole in modified gravity theories. These results represent an important first step in understanding the altered dynamics of an EMRI under modified gravity. Such dynamics will ultimately leave detectable signatures in the gravitational waves emitted by these systems. In the next chapter, we discuss potential directions for future research to build on these

findings.

Chapter 8

Outlook

Having identified the parameter space for geodesic bound orbits, an intriguing next step is to visualize individual bound geodesic orbits within these regions of phase space. By selecting appropriate initial conditions and solving Hamilton's equations numerically, it becomes possible to directly explore the orbital dynamics predicted by our model. Such visualizations could be instrumental in identifying dynamical features, such as resonances. Moreover, analyzing whether shifts in the positive island regions of the effective potential correspond to observable changes in the geodesic orbits themselves would provide a valuable consistency check.

A compelling objective is to identify resonant orbits within the integrable framework of General Relativity and examine how these orbits are influenced by modified gravity theories. Investigating the perturbative effects of the coupling constants α_{sGB} and α_{dCS} on these resonant orbits could uncover chaotic imprints of modified gravity on orbital dynamics. These findings could not only enhance our theoretical understanding but also guide the search for observational signatures of beyond-GR physics in gravitational wave data.

Another promising direction for future work lies in applying the Marsden-Weinstein phase space reduction to the Kerr-like spacetimes of EMRI systems. We have now implicitly done a phase space reduction using our effective potential framework, explicitly following the original methodology introduced by Jerrold Marsden and Alan Weinstein in 1974 could provide deeper insights into the underlying dynamics. Formalizing this reduction has the potential to illuminate previously hidden structures in the phase space, clarify the interplay of conserved quantities, and refine our understanding of geodesic motion. Ultimately, these insights could enhance waveform models by providing a more detailed characterization of the phase space trajectories relevant to gravitational wave signatures.

In summary, this work establishes a foundation for a meaningful interplay between theory and observation, providing a pathway to advance our understanding of gravitational physics and its potential extensions. The rigorous mathematical tools developed in this work offer a robust framework for exploring these extensions.

Bibliography

[1] D. Howard, J. Stachel, and Wolfgang Drechsler. "Einstein and the History of General Relativity". In: *Physics Today* 44.2 (Feb. 1991), pp. 96–98. ISSN: 0031-9228. DOI: 10.1063/1.2809998.

[2] Clifford M. Will. "The Confrontation between General Relativity and Experiment". In: *Living Reviews in Relativity* 17.1 (June 2014). ISSN: 1433-8351. DOI: 10.12942/lrr-2014-4.

[3] Matthew D. Schwartz. *Quantum Field Theory and the Standard Model*. Cambridge University Press, 2013. ISBN: 9781108985031.

[4] Falk Neugebohrn. "Renormalization and Effective Actions for General Relativity". In: (Apr. 2007). arXiv:0704.3205 [hep-th]. URL: http://arxiv.org/abs/0704.3205.

[5] John F Donoghue, Mikhail M Ivanov, and Andrey Shkerin. "EPFL Lectures on General Relativity as a Quantum Field Theory". en. In: (2017).

[6] A. Petrov. *Introduction to Modified Gravity*. SpringerBriefs in Physics. Springer Cham, 2020. ISBN: 978-3-030-52862-1.

[7] Stephon H S Alexander and S James Gates. "Can the string scale be related to the cosmic baryon asymmetry?" In: *Journal of Cosmology and Astroparticle Physics* 2006.06 (June 2006), pp. 018–018. ISSN: 1475-7516. DOI: 10.1088/1475-7516/2006/06/018.

[8] David G. Boulware and Stanley Deser. "String Generated Gravity Models". In: *Phys. Rev. Lett.* 55 (1985), p. 2656. DOI: 10.1103/PhysRevLett.55.2656.

[9] P. Kanti et al. "Dilatonic black holes in higher curvature string gravity". In: *Physical Review D* 54.8 (Oct. 1996), pp. 5049–5058. ISSN: 1089-4918. DOI: 10.1103/physrevd.54.5049.

[10] Victor Taveras and Nicolás Yunes. "Barbero-Immirzi parameter as a scalar field: K-inflation from loop quantum gravity?" In: *Physical Review D* 78.6 (Sept. 2008). ISSN: 1550-2368. DOI: 10.1103/physrevd.78.064070.

[11] B. P. Abbott et al. "Observation of Gravitational Waves from a Binary Black Hole Merger". In: *Physical Review Letters* 116.6 (Feb. 2016). ISSN: 1079-7114. DOI: 10.1103/physrevlett.116.061102.

[12] Pau Amaro-Seoane et al. *Laser Interferometer Space Antenna*. 2017. arXiv: 1702.00786 [astro-ph.IM]. URL: https://arxiv.org/abs/1702.00786.

[13] Michele Maggiore et al. "Science case for the Einstein telescope". In: *Journal of Cosmology and Astroparticle Physics* 2020.03 (Mar. 2020), pp. 050–050. ISSN: 1475-7516. DOI: 10.1088/1475-7516/2020/03/050.

[14] Jonathan Gair et al. "Space-Based Gravitational Wave Observatories". In: *Handbook of Gravitational Wave Astronomy*. Ed. by Cosimo Bambi, Stavros Katsanevas, and Konstantinos D. Kokkotas. Singapore: Springer Singapore, 2020, pp. 1–71. ISBN: 978-981-15-4702-7. DOI: 10.1007/978-981-15-4702-7_3-1.

[15] Zhen Pan et al. *Resonant dynamics of extreme mass-ratio inspirals in a perturbed Kerr spacetime*. 2023. arXiv: 2306.06576 [gr-qc]. URL: https://arxiv.org/abs/230

[16] Tanja Hinderer and Eanna E. Flanagan. "Two timescale analysis of extreme mass ratio inspirals in Kerr. I. Orbital Motion". In: *Phys. Rev. D* 78 (2008), p. 064028. DOI: 10.1103/PhysRevD.78.064028. arXiv: 0805.3337 [gr-qc].

[17] Stephon Alexander and Nicolás Yunes. "Chern–Simons modified general relativity". In: *Physics Reports* 480.1–2 (Aug. 2009), pp. 1–55. ISSN: 0370-1573. DOI: 10.1016/j.physrep.2009.07.002.

[18] S. Nojiri, S. D. Odintsov, and V. K. Oikonomou. "Ghost-free Gauss-Bonnet theories of gravity". In: *Phys. Rev. D* 99 (4 Feb. 2019), p. 044050. DOI: 10.1103/PhysRevD.99.044050. URL: https://link.aps.org/doi/10.1103/PhysRevD.99.0

[19] K. S. Stelle. "Renormalization of higher-derivative quantum gravity". In: *Phys. Rev. D* 16 (4 Aug. 1977), pp. 953–969. DOI: 10.1103/PhysRevD.16.953.

[20] Georgios Lukes-Gerakopoulos and Vojtěch Witzany. "Non-linear effects in EMRI dynamics and their imprints on gravitational waves". In: (Mar. 2021). DOI: 10.1007/978-981-15-4702-7_42-1. arXiv: 2103.06724 [gr-qc].

[21] Jeandrew Brink. "Spacetime encodings. II. Pictures of integrability". In: *Phys. Rev. D* 78 (10 Nov. 2008), p. 102002. DOI: 10.1103/PhysRevD.78.102002.

[22] Mikio Nakahara. *Geometry, topology and physics*. Institute of physics publishing, 2003. ISBN: 0 7503 0606 8.

[23] John M. Lee. *Introduction to Smooth Manifolds*. Springer New York, 2003. ISBN: 978-0-387-21752-9. URL: https://doi-org.proxy.library.uu.nl/10.1007/978-0-38

[24] Ana Cannas Silva. *Lectures on Symplectic Geometry*. Springer Berlin, 2004. ISBN: 978-3-540-45330-7. URL: https://doi-org.proxy.library.uu.nl/10.1007/978-3-54

[25] Jerrold Marsden Ralph Abraham. *Foundations of Mechanics*. Addison-Wesley Publishing Company, 1978. ISBN: 8-8053-01 02-X.

[26] H. Goldstein, C.P. Poole, and J.L. Safko. *Classical Mechanics*. Addison Wesley, 2002. ISBN: 9780201657029. URL: https://books.google.nl/books?id=tJCuQgAACA

[27] A. Zee. *Group theory in a nutshell for physicists*. In a nutshell. Princeton: Princeton University Press, 2016. ISBN: 978-0-691-16269-0.

[28] Bozidar Jovanovi´c. "What are completely integrable Hamilton systems". In: *Teaching of Mathematics* 14.1 (2011), pp. 1–14.

[29] V.I. Arnold et al. *Mathematical Aspects of Classical and Celestial Mechanics*. Encyclopaedia of Mathematical Sciences. Springer Berlin Heidelberg, 2007. ISBN: 9783540489269. URL: https://books.google.nl/books?id=25iQQvHe9awC.

[30] V. I. Arnold. *Mathematical Methods of Classical Mechanics*. Springer New York, 1989. ISBN: 978-0-387-96890-2. URL: https://doi-org.proxy.library.uu.nl/10.100

[31] Jerrold Marsden and Alan Weinstein. "Reduction of symplectic manifolds with symmetry". In: *Reports on Mathematical Physics* 5.1 (1974), pp. 121–130. ISSN: 0034-4877. DOI: https://doi.org/10.1016/0034-4877(74)90021-4. URL: https://www.sciencedirect.com/science/article/pii/0034487774900214.

[32] J.M. Souriau. *Structure of Dynamical Systems: A Symplectic View of Physics*. Progress in Mathematics. Birkhäuser Boston, 1997. ISBN: 9780817636951. URL: https://books.google.nl/books?id=4tBrbryIKQAC.

[33] Charles-Michel Marle Paulette Libermann. *Symplectic Geometry and Analytical Mechanics*. Springer Dordrecht, 1987. ISBN: 978-90-277-2438-0. URL: https://doi.org/10.1007/978-94-009-3807-6.

[34] V I Arnol'd. "PROOF OF A THEOREM OF A. N. KOLMOGOROV ON THE INVARIANCE OF QUASI-PERIODIC MOTIONS UNDER SMALL PERTURBATIONS OF THE HAMILTONIAN". In: *Russian Mathematical Surveys* 18.5 (Oct. 1963), p. 9. DOI: 10.1070/RM1963v018n05ABEH004130. URL: https://dx.doi.org/10.1070/RM1963v018n05ABEH004130.

[35] A N Kolmogorov. "On conservation of conditionally periodic motions for a small change in Hamilton's function". In: *Dokl. Akad. Nauk SSSR* 98 (1954), pp. 527–530. URL: https://cds.cern.ch/record/430016.

[36] J Möser. "On invariant curves of area-preserving mappings of an annulus". In: *Nachr. Akad. Wiss. Göttingen, II* (1962), pp. 1–20. URL: https://cds.cern.ch/record/4

[37] Heinz Hanßmann. "Non-degeneracy conditions in kam theory". en. In: *Indagationes Mathematicae* 22.3-4 (Dec. 2011), pp. 241–256. ISSN: 00193577. DOI: 10.1016/j.indag.2011.09.005. URL: https://linkinghub.elsevier.com/retrieve/ (visited on 06/26/2024).

[38] Sean M. Carroll. *Spacetime and Geometry: An Introduction to General Relativity*. Cambridge University Press, 2019. ISBN: 9781108770385.

[39] The Event Horizon Telescope Collaboration et al. "First M87 Event Horizon Telescope Results. I. The Shadow of the Supermassive Black Hole". In: *The Astrophysical Journal Letters* 875.1 (Apr. 2019), p. L1. DOI: 10.3847/2041-8213/ab0ec7.

[40] Ovidiu Cristinel Stoica. *An Exploration of the Singularities in General Relativity*. 2012. arXiv: 1207.5303 [gr-qc].

[41] Iberê Kuntz and Roberto Casadio. "Singularity avoidance in quantum gravity". In: *Physics Letters B* 802 (2020), p. 135219. ISSN: 0370-2693. DOI: https://doi.org/10.1016/j.physletb.2020.135219.

[42] M. Ostrogradsky. "Mémoires sur les équations différentielles, relatives au problème des isopérimètres". In: *Mem. Acad. St. Petersbourg* 6.4 (1850), pp. 385–517.

[43] Hector O. Silva et al. "Stability of scalarized black hole solutions in scalar-Gauss-Bonnet gravity". In: *Physical Review D* 99.6 (Mar. 2019). ISSN: 2470-0029. DOI: 10.1103/physrevd.99.064011.

[44] Marek Liška, Robie A. Hennigar, and David Kubizňák. "No logarithmic corrections to entropy in shift-symmetric Gauss-Bonnet gravity". In: *Journal of High Energy Physics* 2023.11 (Nov. 2023). ISSN: 1029-8479. DOI: 10.1007/jhep11(2023)195. URL: http://dx.doi.org/10.1007/JHEP11(2023)195.

[45] Fech Scen Khoo et al. *Quasinormal modes of rotating black holes in shift-symmetric Einstein-scalar-Gauss-Bonnet theory*. 2024. arXiv: 2412.09377 [gr-qc]. URL: https://arxiv.org/abs/2412.09377.

[46] Félix-Louis Julié and Emanuele Berti. "Post-Newtonian dynamics and black hole thermodynamics in Einstein-scalar-Gauss-Bonnet gravity". In: *Phys. Rev. D* 100 (10 Nov. 2019), p. 104061. DOI: 10.1103/PhysRevD.100.104061. URL: https://link.aps.org/doi/10.1103/PhysRevD.100.104061.

[47] M. Crisostomi et al. "Beyond Lovelock gravity: Higher derivative metric theories". In: *Phys. Rev. D* 97 (4 Feb. 2018), p. 044034. DOI: 10.1103/PhysRevD.97.044034.

[48] R. Jackiw and S.-Y. Pi. "Chern-Simons modification of general relativity". In: *Physical Review D* 68.10 (Nov. 2003). ISSN: 1089-4918. DOI: 10.1103/physrevd.68.104012

[49] Tristan L. Smith et al. "Effects of Chern-Simons gravity on bodies orbiting the Earth". In: *Physical Review D* 77.2 (Jan. 2008). ISSN: 1550-2368. DOI: 10.1103/physrevd.77.024015.

[50] Christopher P. L. Berry et al. *The unique potential of extreme mass-ratio inspirals for gravitational-wave astronomy*. 2019. arXiv: 1903.03686 [astro-ph.HE]. URL: https://arxiv.org/abs/1903.03686.

[51] Fintan D. Ryan. "Gravitational waves from the inspiral of a compact object into a massive, axisymmetric body with arbitrary multipole moments". In: *Phys. Rev. D* 52 (10 Nov. 1995), pp. 5707–5718. DOI: 10.1103/PhysRevD.52.5707.

[52] W Schmidt. "Celestial mechanics in Kerr spacetime". In: *Classical and Quantum Gravity* 19.10 (Apr. 2002), pp. 2743–2764. ISSN: 0264-9381. DOI: 10.1088/0264-9381/19/10/314. URL: http://dx.doi.org/10.1088/0264-9381/19/10/314

[53] Pablo A. Cano and Alejandro Ruipérez. "Leading higher-derivative corrections to Kerr geometry". In: *Journal of High Energy Physics* 2019.5 (May 2019). ISSN: 1029-8479. DOI: 10.1007/jhep05(2019)189.

[54] Robert M. Wald. *Introduction to Gravitational Self-Force*. 2009. arXiv: 0907.0412 [gr-qc]. URL: https://arxiv.org/abs/0907.0412.

[55] Francisco M. Blanco and Éanna É. Flanagan. "Particle Motion under the Conservative Piece of the Self-Force is Hamiltonian". In: *Physical Review Letters* 130.5 (Feb. 2023). ISSN: 1079-7114. DOI: 10.1103/physrevlett.130.051201. URL: http://dx.doi.org/10.1103/PhysRevLett.130.051201.

[56] Caroline B. Owen, Nicolás Yunes, and Helvi Witek. "Petrov type, principal null directions, and Killing tensors of slowly rotating black holes in quadratic gravity". In: *Physical Review D* 103.12 (June 2021). ISSN: 2470-0029. DOI: 10.1103/physrevd.103.124057. URL: http://dx.doi.org/10.1103/PhysRevD.1

[57] James M. Bardeen, William H. Press, and Saul A. Teukolsky. "Rotating Black Holes: Locally Nonrotating Frames, Energy Extraction, and Scalar Synchrotron Radiation". In: 178 (Dec. 1972), pp. 347–370. DOI: 10.1086/151796.

[58] Scott E. Perkins et al. "Improved gravitational-wave constraints on higher-order curvature theories of gravity". In: *Physical Review D* 104.2 (July 2021). ISSN: 2470-0029. DOI: 10.1103/physrevd.104.024060.

[59] Hector O. Silva et al. "Astrophysical and Theoretical Physics Implications from Multimessenger Neutron Star Observations". In: *Physical Review Letters* 126.18 (May 2021). ISSN: 1079-7114. DOI: 10.1103/physrevlett.126.181101. URL: http://dx.doi.org/10.1103/PhysRevLett.126.181101.

[60] M. J. Reid and A. Brunthaler. "The Proper Motion of Sagittarius A*. II. The Mass of Sagittarius A*". In: *The Astrophysical Journal* 616.2 (Dec. 2004), p. 872. DOI: 10.1086/424960.